Molecular Breeding (2026) 46:108
https://doi.org/10.1007/s11032-026-01728-8

Molecular Breeding

RESEARCH

Elucidating the genetic architecture of yield components in pyramidale wheat (*Triticum turgidum* L.): a comparative approach using QTL analysis and genomic selection

Tiantian Chen[1] · Kazusa Nishimura[2] · Kazuki Murata[1] · Takanori Yoshikawa[1] · Kyoka Nagasaka[1] · Takahiro Maki[1] · Ko Motoki[2] · Yu Kinoshita[3] · Yu Iwahashi[1] · Hiromo Inoue[1] · Tetsuya Nakazaki[4] · Ryohei Nakano[1]

Received: 19 February 2026 / Accepted: 4 October 2026 / Published online: 15 October 2026
© The Author(s) 2026

Abstract

Wheat grain yield is determined by three primary components, one of which is grain number per spike (GPS; or spike fertility). GPS is further determined by spikelet number per spike (StPS) and grain number per spikelet (GPSt). TN28, a pyramidale wheat accession, produces up to five grains per spikelet, substantially exceeding the number in typical cultivars. To elucidate the genetic architecture underlying TN28's superior traits and determine the optimal breeding strategy for trait introgression, we evaluated yield-related traits in a biparental F_2 population derived from TN28 × Langdon across three environments over two years using quantitative trait locus (QTL) mapping and genomic selection (GS). QTL analysis using two mapping approaches detected no stable QTLs other than known flowering genes, indicating that TN28's yield-related traits cannot be reliably introgressed via single- or few-marker selection. Conversely, GS using five prediction models demonstrated potential for accumulating favorable minor-effect alleles. The ridge regression model exhibited optimal performance for GPSt-related traits, with the top 20% of individuals selected on the basis of genomic estimated breeding values (GEBVs) achieving approximately 9% higher grain number per spikelet at the basal section (GPStB) and 7% higher grain number per spike (GPS) relative to the population mean. These results support that QTL mapping is effective for traits controlled by a single major-effect gene, whereas GS offers a more powerful strategy for traits controlled by multiple minor-effect genes. This study suggests that TN28's superior yield-related traits may arise from the cumulative contribution of numerous minor-effect genes and establishes GS as the preferred tool for their improvement in breeding programs.

Keywords Durum wheat · Pyramidale · Spike fertility · QTL · Genomic selection

Extended author information available on the last page of the article

Introduction

Wheat (*Triticum* spp.), one of the three main staple crops worldwide, accounts for approximately 35% of the global daily intake of carbohydrates and proteins (Ogbonnaya et al. 2013). However, the rapid population growth has posed a considerable challenge to global food security. In 2022, an estimated 29.6% of the global population (2.4 billion people) faced moderate or severe food insecurity. This is roughly 122 million more people than in 2019, the year before the COVID-19 pandemic (FAO et al. 2023). Furthermore, between 2003 and 2019, a 21% increase in global population was accompanied by a 10% decline in per-capita cropland area (Potapov et al. 2022). Although cropland expansion has partially offset this pressure, replacing natural vegetation with croplands has exacerbated biodiversity loss and climate change (Hasan et al. 2020; Liu et al. 2024). Under these circumstances, enhancing wheat productivity has become imperative for ensuring sustainable food security.

Wheat grain yield is determined by three primary components: number of spikes per unit area, grain number per spike (GPS), and thousand-grain weight. These components can be further broken down into subcomponents; for example, GPS (spike fertility) is determined by grain number per spikelet (GPSt) and spikelet number per spike (StPS). Increasing any of the grain yield components would contribute to the final grain yield. Importantly, grain yield components typically exhibit higher heritability than grain yield itself (Zhang et al. 2018). Studies have identified quantitative trait loci (QTLs) associated with yield components (Chen et al. 2017; Lin et al. 2021). For instance, the gene *Grain Number Increase 1* (*GNI1*), which underlies a QTL for GPSt, was identified on chromosome 2A (Sakuma et al. 2019). In parallel, *WHEAT ORTHOLOG OF APO1* (*WAPO1*), located on the long arm of chromosome 7A, was identified as the causal gene controlling StPS (Kuzay et al. 2019, 2022; Muqaddasi et al. 2019). *WAPO1* was discovered through QTL mapping and genome-wide association studies, followed by validation across diverse genetic backgrounds using functional genetic markers. Beyond the direct determinants of grain number and weight, flowering time also exerts a profound influence on spike architecture and yield components. In wheat, flowering time is regulated primarily by the photoperiod response genes (*Ppd-1*), vernalization requirement genes (*Vrn-1*, *Vrn-2*, *Vrn-3*), and earliness per se (*Eps*) loci, which together determine the timing and duration of reproductive development (Worland 1996; Yan et al. 2003; Beales et al. 2007). For instance, several studies have reported that allelic variation at *Ppd-1* affects the dynamics of spikelet and floret primordia initiation and ultimately grain set per spike (Boden et al. 2015; Ochagavía et al. 2018; Prieto et al. 2018). These findings underscore that flowering time cannot be treated as independent of yield component traits, and that flowering time loci merit consideration alongside spike-specific QTLs in the genetic dissection of wheat yield. Nevertheless, despite the identification of genes such as *GNI1*, *WAPO1*, and key flowering time loci, most reported yield-related QTLs have not been effectively utilized in marker-assisted selection (MAS) because their causal genes remain unknown and their phenotypic effects are not sufficiently large. MAS has several additional constraints, including: i) biased estimates of QTL effects resulting from a small population size (Xu 2003); and ii) difficult transferability of QTL effects across populations and environments because of gene × gene (epistatic) and

genotype × environment (G × E) interactions (Xu and Crouch 2008; Bernardo 2008). These constraints have driven the development of alternative breeding strategies that can simultaneously account for numerous minor-effect loci distributed across the genome, thereby improving the prediction of breeding values and genetic gains for complex yield-related traits.

Genomic selection (GS), first proposed by Meuwissen et al. (2001), has the potential to overcome the constraints of conventional MAS. In contrast to MAS, which relies solely on markers significantly associated with target traits, GS employs all genome-wide markers simultaneously to predict genomic estimated breeding values (GEBVs). Selection is then based on the predicted values. In this context, GS can be viewed as MAS without prior QTL mapping (Bernardo 2014, 2020), enabling the capture of both major- and minor-effect alleles underlying complex traits. Advances in sequencing and high-throughput genotyping have facilitated the widespread application of GS across various crops, targeting grain yield as well as resistance to biotic and abiotic stresses (Anilkumar et al. 2022). In addition to improving selection accuracy, GS also accelerates breeding cycles and lowers phenotyping costs. Therefore, it is a promising tool for improving quantitative traits in the era of modern biotechnology. Recent advances in GS have enabled the selection of yield-related traits, highlighting the potential to integrate minor-effect genes into breeding programs. Consequently, to achieve more efficient genetic improvement of yield-related traits, it is necessary to re-evaluate genetic resources, identify additional major-effect genes suitable for MAS, and adopt strategies to effectively utilize these genetic resources through techniques such as GS for minor-effect genes.

From this perspective, in this study, we focus on genetic resources that have not been widely utilized to date, particularly tetraploid wheat (*Triticum turgidum* L.), and advance genetic analyses of yield-related traits. Through cultivation and observation of multiple tetraploid wheat cultivars in the field, we found that TN28, a tetraploid pyramidale wheat accession (*T. turgidum* ssp. *durum,* conv. *pyramidale*), produced an exceptionally high number of grains. TN28 has been observed to produce up to five grains per spikelet at the basal section of the spike, significantly exceeding the typical two to three grains in tetraploid wheat (Shitsukawa et al. 2009). However, despite apparent morphological differences from durum wheat, there has been no research on its yield components, although there have been studies on its heading date (HD) and chromosome doubling capacity (Nishimura et al. 2018; Matsuoka and Mori 2020). Consequently, the identification and exploitation of genes controlling the high GPSt phenotype in TN28 present a valuable opportunity to enhance wheat yield potential.

The genetic architecture underlying TN28's superior traits remains unknown—whether it is controlled by major-effect loci amenable to MAS or minor-effect loci requiring GS. Thus, in this study, we sought to elucidate the genetic factors underlying TN28's high yield potential and to determine the optimal breeding strategy for trait introgression. Multiple yield-related traits, including GPSt, were examined over two years across three environments using a biparental F_2 population derived from TN28 × Langdon (LDN) (*T. turgidum* ssp. *durum*). We employed a dual approach: first, we performed QTL analysis to identify potential major-effect loci, and then, we implemented GS to assess whether these traits are better captured by genomic predic-

tion models. Through this comparative strategy, we established an optimal methodology for utilizing TN28's valuable traits in wheat breeding programs.

Materials and methods

Plant materials and growth conditions

An F_2 population was developed from a cross between TN28 and LDN. TN28 harbors the photoperiod-insensitive *Ppd-A1* allele (Nishimura et al. 2018), an ortholog of the pseudo-response regulator (*PRR*) family member *PRR37*, contributing to flowering regulation (Beales et al. 2007; Guo et al. 2010) and StPS in wheat (Boden et al. 2015). LDN harbors the photoperiod-sensitive *Ppd-A1* allele (Nguyen et al. 2015).

The F_2 population developed from this cross and its parental lines were cultivated for two years across three environments during the 2020–2021 and 2022–2023 growing seasons in the same greenhouse at the Experimental Farm of the Graduate School of Agriculture, Kyoto University (34°44′02.4″N, 135°50′16.2″E). During the 2020–2021 growing season, this F_2 population was cultivated under a single conventional fertilization condition ($n = 144$; hereinafter, this F_2 population is referred to as 20A). During the 2022–2023 growing season, plots with different fertilizer application rates were established to expose the F_2 population to contrasting fertilization conditions. Then, the parental lines and the F_2 population were cultivated under two fertilization conditions: conventional ($n = 198$; 22AC) and additional ($n = 168$; 22AF). For 22AF, 30 kg of ammonium sulfate per hectare was applied, corresponding to 0.3793 kg per 26.55 m^2 plot. 22AF was fertilized once, on 3rd March 2023, receiving nitrogen a 21%. Hereinafter, these cultivation environments will be referred to as 20A, 22AC, and 22AF, respectively.

The F_2 population across three environments and the two parental lines were treated equally before transplanting: First, seeds were germinated at 20 °C under 24-h day-length conditions on wet filter paper for 2 days. Subsequently, they were transplanted into 2 cm × 2 cm cell trays. After growing at 20 °C in a phytotron under natural light conditions for 10 days, the seedlings were transplanted into the greenhouse at a spacing of 1 m between rows and 15 cm between individuals. The dates for seed sowing and transplanting are summarized in Table S1. The 22AC and 20A environments were cultivated under standard conditions in accordance with established growth protocols.

To measure nitrogen levels in greenhouse soil during the 2022–2023 growing season, each environment was split into three blocks, and soils from six randomly selected locations within each block were sampled before and after nitrogen fertilization. Sampling before fertilization was performed one day before nitrogen application, whereas sampling after fertilization was performed 11 days after nitrogen application. Electrical conductivity (EC) and pH values were measured for each block, and the Student's *t*-test was used to evaluate differences between 22AC and 22AF trials.

Phenotypic evaluation of F_2 population and its parental lines

Seven yield-related traits were examined in the F_2 population across three environments (Table S2). We investigated spike-related traits, including StPS, GPS, and GPSt. These traits were determined by investigating five randomly sampled spikes from an individual plant. StPS was measured by averaging the number of spikelets per spike. GPS was measured by averaging the number of grains per spike. GPSt was obtained by GPS/StPS. Moreover, to evaluate variation in GPSt along the wheat spike, each spike was divided into three regions — apical (A), central (C), and basal (B) — based on the total spikelet number per spike (Table S3), following the method by Mizuno et al. (2021). GPSt was then calculated separately for each region, yielding GPSt at the apical (GPStA), central (GPStC), and basal (GPStB) region of the spike. In addition to spike-related traits, HD was determined as the number of days from transplant to the emergence of the tip of the first spike beyond the flag leaf, assessed for each plant. Data analysis was performed using a custom R script. For the parental lines, the maximum, minimum, and mean phenotypic values and the standard deviation of measured traits were calculated. Then, their means were compared by the Student's *t*-test between the two parental lines. For progenies, the maximum, minimum, and mean phenotypic values and the standard deviation of measured traits were calculated. Besides, the normality of the phenotypic distribution for each trait was tested using the Shapiro–Wilk test. When the *P*-value was less than 0.05, the distribution was considered to deviate significantly from a normal one. Furthermore, differences in mean phenotypic values across the three environments were evaluated using analysis of variance (ANOVA), followed by the Tukey test. Broad-sense heritability was not estimated in this study. Because each F_2 population was evaluated in a single environment and the environmental variance could only be inferred from a small number of non-segregating parental plants, reliable variance-component estimates could not be obtained under the present design.

DNA extraction and genome-wide genotyping by MIG-seq

The F_2 population across three environments and the parental lines were genotyped using multiplexed inter-simple sequence repeats genotyping by sequencing (MIG-seq), a PCR-based high-throughput genotyping method described in Nishimura et al. (2022). DNAs from 20A were extracted from the leaves of individuals using the method reported by Zheng et al. (1995). DNAs from 22AC and 22AF were extracted using a DNA extraction buffer containing PVPP developed by Nishimura et al. (2024). MIG-seq libraries for the F_2 population were sequenced on an Illumina NovaSeq X plus.

To generate variant call format (VCF) files, 151 bp paired-end data were trimmed and filtered using fastp v0.23.4 (Chen et al. 2018) with the following parameters '-q 20 -n 10 -f 17 -F 17'. Using SNAP (version 2.0.0) (Zaharia et al. 2011), we mapped the trimmed reads to the reference genome of durum wheat cv. Svevo (Maccaferri et al. 2019). This was followed by sorting and indexing the aligned reads in SAMtools 1.18 using HTSlib 1.17 (Li et al. 2009). Variant call was performed using the bcftools (version 1.18) (Li et al. 2009) mpileup command with the '-d 1,000,000' option and

the call command with the '-mv' option to create a VCF file. Then, we filtered the VCF file using VCFtools (version 0.1.16) (Danecek et al. 2011) with parameters: –max-missing 0.7 –minDP 5 –max-alleles 2 –min-alleles 2 –maf 0.1.

QTL analysis of yield-related traits

To enable straightforward comparison of QTL results across the three environments, we generated a VCF file that contains all individuals evaluated in the 220A, 20AC, and 20AF trials. Using this filtered VCF file, we constructed a single linkage map, enabling the analysis of phenotypic data from the three environments on the same map. The linkage map was created with Lep-Map3 (version 0.4), as described in Rastas (2017). First, the filtered VCF file, along with a pedigree text file, was imputed using the ParentCall2 module to call parental genotypes. Then, they were filtered using the Filtering2 module to exclude homozygous markers and distorted markers with a data tolerance for segregation distortion of 0.000001. Next, the filtered markers were assigned to linkage groups using the SeparateChromosomes2 module with the parameters: lodLimit = 14 numThreads = 10. Finally, markers within each LG (linkage group) were ordered by the OrderMarkers2 module using Morgan's mapping function, with the following parameters: sexAveraged = 1 grandparentPhase = 1 outputPhasedData = 1. The constructed linkage maps were confirmed by plotting the markers on both physical and genetic maps.

QTL mapping was conducted in R/qtl (Broman et al. 2003) using the phenotypic values for each trait from each environment. Genotype probabilities were first calculated at 1-cM intervals across the genome using the "calc.genoprob" function, providing the basis for subsequent interval mapping analyses. Both simple interval mapping (SIM) and composite interval mapping (CIM) were performed using the Haley–Knott regression (Haley and Knott 1992). SIM was implemented in the "scanone" function, whereas CIM was implemented using the cim function with five marker covariates. To determine genome-wide significance thresholds, 1,000 permutation tests were carried out (Churchill and Doerge 1994), and QTLs exceeding the 5% significance threshold were recorded. Significant peaks detected by both SIM and CIM were summarized, and profiles of the logarithm of the odds (LOD) score were plotted with their corresponding permutation-based thresholds. All QTL results, including LOD score, peak LOD score on the genetic map position, and closest trait-associated markers, were summarized for downstream analyses. Following the identification of putative QTLs, QTL effect and phenotypic variance explained (PVE) by QTL for corresponding traits were estimated using the "fitqtl" function. For QTLs detected by both SIM and CIM, the peak position of the QTL detected by SIM was used for estimation. If multiple QTLs were detected for a trait within an environment, "fitqtl" was used to test a model containing both QTLs. The confidence interval (CI) for each QTL was determined by the 1.8–LOD interval (Manichaikul et al. 2006). The physical position of the CI for each QTL was determined by the positions of flanking markers on the physical map. QTLs with partially or completely overlapping confidence intervals were considered co-located; when co-located QTLs were detected for more than two traits, they were designated as common QTLs, potentially representing pleiotropic or closely linked loci. QTLs were named in accordance with

the Rules of Genetic Nomenclature for wheat (Boden et al. 2023). The abbreviations "Yld" and "ku" were adopted for "Yield" and "Kyoto University", and other abbreviations are described in Table S2.

Comparative analysis with known genes for yield-related traits

For previously reported important genes for spike-related traits *WAPO1 and GNI-A1*, we investigated their genomic sequences to identify polymorphisms between the two parental lines, TN28 and LDN. DNAs extracted from the two parental lines were sent to BGI Japan, where libraries were constructed and sequenced using DNB-seq with 150 bp paired-end. reads The sequenced reads were filtered by fastp with the following options: '-q 20 -n 10 -l 35'. Filtered reads were mapped to Svevo v1.0 using SNAP aligner, sorted with SAMtools sort, and converted to BAM format. Then, the physical regions of these genes in the resequenced genomes of two parental accessions, TN28 and LDN, were compared. For *GNI-A1*, sequences were compared by viewing the BAM files of the whole genome resequencing data in an Integrative Genomics Viewer (Robinson et al. 2017) (IGV_2.8.0). For *WAPO1*, sequence alignment analysis was performed using CLC Genomics Workbench (version 24.0.1) with sequences of TN28, LDN, and PI 41025 (*T. turgidum* subsp. *dicoccum*).

Marker development and QTL confirmation

To validate the genotype of the MIG-seq-derived genetic marker associated with major-effect QTLs, a pair of InDel (Insertion-Deletion) markers was developed on the basis of polymorphisms identified in the vicinity of the QTL region using whole-genome resequencing data from the two parental lines (Table S4). These InDel markers were used to genotype the F_2 population across all three environments for QTL confirmation. Amplification was carried out in a 10 µL reaction mixture containing 5 µL of KOD One, 2 µL of 2.5 µM forward primer, 2 µL of 2.5 µM reverse primer, and 1 µL of genomic DNA. Amplification was performed at 98 °C for 1 min, followed by 35 cycles of 98 °C for 5 s, 60 °C for 1 s, and 68 °C for 1 s, with a final extension at 68 °C for 5 min. PCR products were electrophoresed on 3% agarose gels. In accordance with the genotyping results, individuals within each environment were categorized as follows: (1) those homozygous for the LDN allele, (2) those homozygous for the TN28 allele, and (3) heterozygous individuals. To examine genotype × environment (G × E) interactions, a two-way analysis of variance (ANOVA) with genotype class and environment (20A, 22 C, or 22 F) as factors was performed across all three genotypic classes. Tukey's honestly significant difference (HSD) test was subsequently applied as a post-hoc procedure to evaluate pairwise phenotypic differences among genotypic classes within each environment.

Candidate genes in the QTL region

To predict candidate genes for major-effect QTLs, whole-genome resequencing data of the two parental lines were compared to identify mutations within the QTL regions of interest. These mutations were functionally annotated with SnpEff (v5.2) (Cingo-

lani et al. 2012) based on the annotation of high-confidence genes in durum wheat cv. Svevo. Their predicted effects were categorized into high, low, and moderate impact. Candidate genes underlying QTLs of interest were identified among high-impact mutations whose predicted functions could be related to the analyzed phenotype.

Genomic selection

Genomic selection scenario

Two possibilities can be considered if stable QTLs are not detected by QTL analysis. The first is that the phenotypic difference between the two parental lines arises from the accumulation of multiple minor-effect genes that are difficult to detect using conventional QTL analysis. The second possibility is that the effect of QTLs varies across environments. We hypothesize that when a trait is controlled by numerous minor-effect genes, genomic prediction models trained in one environment can predict the trait in other environments. To test this hypothesis, we evaluated whether genomic prediction could predict data across environments using F_2 data from all three trials (Fig. S1). One environment was used as the training population (TP) to construct a prediction model using its genotypic and phenotypic data. Then, GEBVs were calculated for the remaining two environments serving as the breeding population (BP), using their genotypic data, with marker effects estimated from TP. This design resulted in six prediction scenarios (e.g., 20A as TP with 22AF as BP, 20A as TP with 22AC as BP, etc.).

Prediction model

To capture a range of genetic architectures, five prediction models with different assumptions for estimating marker effects were adopted. The five models were developed using packages in R: ridge regression (RR), least absolute shrinkage and selection operator (LASSO), genomic best linear unbiased predictor (GBLUP), random forest (RF), and extreme learning machine (ELM). RR and LASSO were implemented using the glmnet package (Tay et al. 2023; Friedman et al. 2010). To fit the regularized regression models, cross-validation was performed using the "cv.glmnet" function with the default tenfold setting (nfolds = 10). The mixing parameter α was set to 0 for RR and 1 for LASSO to specify the penalty type. GBLUP was conducted using Bayesian methods from the BGLR package (Pérez and De Los Campos 2014). A reproducing kernel Hilbert space (RKHS) was chosen as the prediction model with a genomic relationship matrix (GRM) provided. GRM was calculated as $GRM = XX^T/p$, where X denotes the standardized marker matrix, and p is the number of markers. RF was implemented using the ranger package (Wright and Ziegler 2017), and ELM was implemented using the elmNNRcpp package (Huang et al. 2006).

Predictive ability of genomic selection

The predictive ability of the five prediction models was assessed using Pearson's correlation between the calculated GEBVs of individuals and the observed phenotypes of individuals in BP. Correlations were calculated for each measured yield-related trait within each prediction scenario. Statistical significance of correlations was assessed using *p*-values of the correlation coefficients. Furthermore, to determine whether the prediction models accurately reflect differences in parental traits, we predicted parental phenotypes based on F_2 population data using the five models described above.

Genomic selection: selection pressure and selection efficiency

To optimize breeding efficiency under GS, the following trade-offs must be considered. Reducing the number of superior lines selected is expected to improve the average value of the selected lines. However, as the number of individuals available for selection decreases, more populations must be prepared to maintain the same number of selected individuals. In this study, we examined 10 selection proportions ranging from 5 to 50% at 5% increments. Within each selection proportion, individuals in BP were ranked by their GEBVs calculated from the prediction model built using TP. Two groups were selected: superior lines (top-ranked individuals) and inferior lines (bottom-ranked individuals). For example, at 10% selection proportion, the top 10% of individuals were designated as superior lines and the bottom 10% as inferior lines. For each selection proportion and prediction scenario, the observed phenotypic values of selected superior and inferior lines were obtained, and the difference between the mean phenotypic values of the two groups was calculated. The Student's *t*-test was used to assess the statistical significance of differences between superior and inferior groups. Furthermore, changes in the phenotypic values of superior lines at a reasonable selection proportion were evaluated and compared with those of the initial BP using the Student's *t*-test.

Results

Phenotypic performance and correlation analysis of yield-related traits in F_2 population

The two parental lines were assessed for seven measured traits among three trials (20A, 22AC, 22AF; Table S5; Fig. S2). TN28, which carries the photoperiod-insensitive *Ppd-A1* allele, consistently exhibited significantly earlier heading than LDN ($p<0.001$ for 20A and 22AF; $p<0.01$ for 22AC), which carries the photoperiod-sensitive *Ppd-A1* allele. Across all trials, TN28 headed approximately 10 days earlier than LDN and exhibited significantly lower StPS than LDN. On the other hand, TN28 was characterized by higher GPS and GPSt than LDN (Table S5; Fig. S2). TN28 produced approximately four more grains per spike than LDN in all trials (an average GPS range of 50.32–62.47 for TN28 and 45.24–58.04 for LDN). However, the

difference was statistically significant only in 22AF. Regarding GPSt-related traits, TN28 exhibited significantly higher values for most traits across all trials except for GPStB in 20A and 22AC and GPStC in 22AC. TN28 showed an average GPSt range of 2.13–2.62, whereas LDN showed an average GPSt range of 1.66–2.07. Based on data averaged across the three environments, TN28 displayed mean values of 1.70, 2.65, and 2.61 for GPStA, GPStC, and GPStB, respectively, whereas LDN showed corresponding mean values of 1.02, 2.22, and 2.10 (Table S5). Although both GPStB and GPStC contributed more than GPStA in both parental lines, as many as five grains per spikelet in the basal section of the spike were observed far more frequently in TN28 than in LDN (Table S6; Fig. S2). Overall, TN28 exhibited stable, earlier heading, lower StPS, and higher GPS and GPSt across the entire spike.

F_2 progenies were assessed for seven measured traits across three evaluation environments. Five randomly selected spikes per individual were examined and those showing obvious infertility in the middle portion were defined as poorly grown and excluded. Individuals retaining fewer than three measurable spikes at harvest were removed, so that the final phenotypic analyses were conducted on 437 F_2 individuals, including 136 in 20A, 166 in 22AC, and 135 in 22AF. The phenotypic distributions of F_2 progenies for the seven traits were assessed using the Shapiro–Wilk test to evaluate normality (Table S5). Whereas HD deviated from normality in all three environments, the remaining six spike-related traits generally exhibited an approximately normal distribution. Transgressive segregation was observed at both extremes of the distributions for all traits, suggesting that both parents contributed alleles that enhance yield (Fig. 1).

The phenotypic distributions of all traits were compared across the three environments, revealing distinct differences across years (Fig. S3; Table S5). The 20A environment, sown and transplanted 12 days earlier, exhibited an approximately 10-day longer duration from transplanting to heading (HD) than the 22AC and 22AF environments. The extended growth period resulted in a higher StPS in 20A (average = 26.79) than in 22AC (average = 24.19) or 22AF (average = 25.12). Furthermore, 20A exhibited higher mean phenotypic values for the remaining five spike-related traits than 22AC and 22AF. For example, the 20A environment exhibited a mean GPS of 66, markedly higher than those observed in 22AC (average = 45.72) and 22AF (average = 44.13). These differences in the six spike-related traits across years may be attributed to variations in climatic conditions and sowing dates (Table S1).

Regarding the 22AC and 22AF environments, 22AC received the same conventional fertilization treatment as 20A, whereas 22AF received nitrogen treatment. To evaluate the effect of nitrogen treatment, two parameters: pH, a measure of soil acidity, and electrical conductivity (EC), a measure of soil salinity, were measured (Table S7). The pH value remained stable at approximately 7 in both environments, before and after treatment. On the other hand, EC values differed between the two environments even before treatment (mean EC of 1.17 for 22AC and 1.39 for 22AF). Following nitrogen treatment, EC significantly increased from 1.39 to 1.86 in 22AF. Thus, 22AF individuals could receive more nutrients than 22AC individuals. When phenotypic distributions were compared between the two environments, within the same year but under different fertilization treatments, significant differences were noted for almost all traits except HD, GPS, and GPStB (Fig. S3; Table S5). Individuals in 22AF

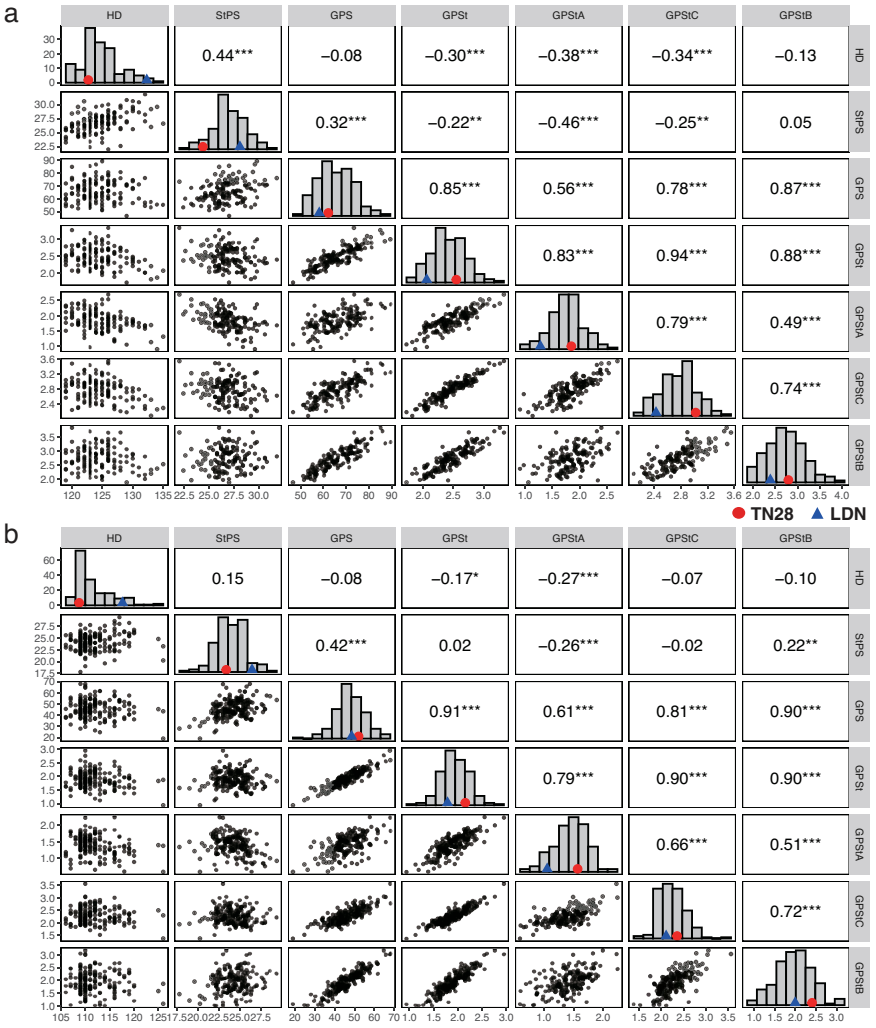


Fig. 1 Frequency distribution of individuals for measured traits and Pearson's correlations among measured traits in F_2 population across three environments. Pairwise Pearson's correlation coefficients (r) were calculated for all seven measured traits for (**a**) 20A, (**b**) 22AC, and (**c**) 22AF environments. The seven measured traits are heading date (HD), spikelet number per spike (StPS), grain number per spike (GPS), grain number per spikelet (GPSt), GPSt at the apical section of the spike (GPStA), GPSt at the central section of the spike (GPStC), and GPSt at the basal section of the spike (GPStB). Diagonal panels show the phenotypic distribution of the F_2 population across three environments and the parental lines. Red dots and blue triangles represent the average of two parental lines, TN28 and Langdon (LDN), respectively. *, **, and *** represent significance at $p<0.05$, $p<0.01$, and $p<0.001$

showed a significantly but slightly higher StPS than individuals in 22AC (24.19 for 22AC and 25.12 for 22AF). However, nitrogen treatment appeared to negatively affect other spike-related traits. 22AF exhibited comparable GPS (45.72 for 22AC and 44.13 for 22AF) and GPStB (1.96 for 22AC and 1.87 for 22AF) values to 22AC,

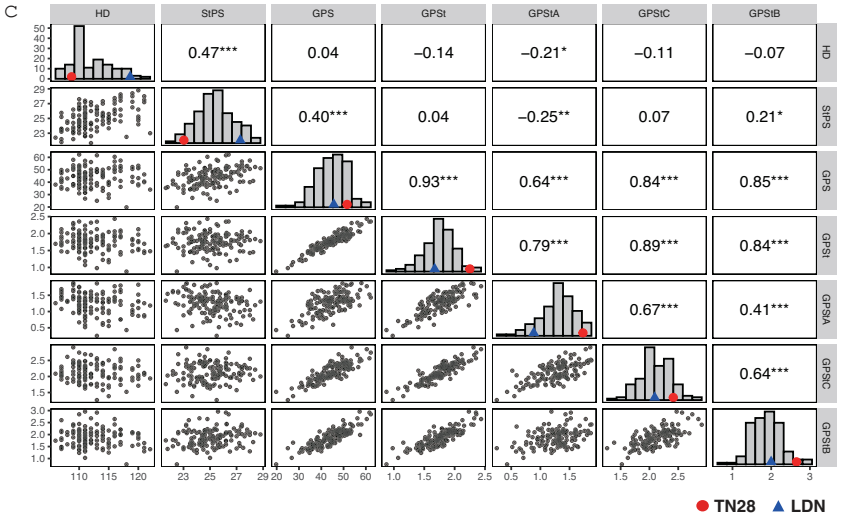


Fig. 1 (continued)

but significantly lower values for other GPSt-related traits. Collectively, these results indicate that 20A, 22AC, and 22AF represent three contrasting environmental conditions, differing in year and/or fertilization treatment, which we could use to examine the consistency of QTL effects in the F_2 population derived from TN28 × LDN.

Phenotypic correlations among measured traits were calculated for each environment. The overall trends were similar across the three environments (Fig. 1). HD showed a significant positive correlation with StPS in the 20A ($r=0.44$) and 22AF ($r=0.47$) environments, but a nonsignificant, weak positive correlation in 22AC ($r=0.15$). On the contrary, HD showed negative correlations with GPSt-related traits, ranging from a statistically significant negative correlation ($r=-0.38$) with GPStA in the 20A environment to a nonsignificant negative correlation ($r=-0.07$) with GPStC in 22AC. The primary yield component, GPS, was composed of StPS and GPSt. Across the three environments, correlations were stronger between GPS and GPSt ($r=0.85$–0.93, $p<0.001$) than between GPS and StPS ($r=0.32$–0.42, $p<0.001$). GPSt was further divided into GPStA, GPStC, and GPStB. Among them, GPStB ($r=0.80$–0.90) had the highest correlation with GPS, followed by GPStC ($r=0.78$–0.84) and GPStA ($r=0.56$–0.64). Taken together, GPStB was suggested to strongly influence total grain number in this environment.

Linkage map construction

To better compare the results of QTL analysis across the three environments, a single linkage map was constructed from all F_2 individuals (Table S8; Figs. S4 and S5). A total of 8,870 unique loci were identified from parents and all individuals in the F_2 population. This marker set was reduced into a set of 6,681 markers by removing those showing significant segregation distortion to construct linkage maps. All linkage maps covered 2934.48 cM in length, including 1489.79 cM (50.7%) for the A

genome and 1444.69 cM (49.3%) for the B genome. The average distance between adjacent loci was 0.44 cM. A total of 2,867 markers were mapped to the A genome (42.9%), each with an average of 409 markers per chromosome, whereas 3,814 markers were mapped to the B genome (57.1%), each with an average of 544 markers per chromosome. Chromosome size ranged from 129.03 cM for chromosome 4B to 247.72 cM for chromosome 3B, with an average of 209.61 cM per chromosome. The number of loci per chromosome ranged from 227 on chromosome 3A to 971 on chromosome 4B, with a mean of 477 loci per chromosome. Chromosome 4B had the highest density of 0.13 cM/locus, whereas chromosome 3A had the lowest average marker density of 1.02 cM/locus. Single-nucleotide polymorphism (SNP) markers were aligned to the physical map of the reference genome of durum wheat cv. Svevo (Maccaferri et al. 2019). The dot plots of physical and genetic distances of markers indicated that recombination frequency near the centromere was suppressed, whereas that near the telomeres was increased, as expected (Fig. S4). These results indicate that we have successfully constructed a genetic linkage map and obtained marker information of sufficient density for QTL analysis.

QTL mapping in single environments

QTL analysis was performed using the single linkage map with SIM and CIM methods (Table 1; Fig. 2a). A total of 22 QTLs were detected for the measured traits. No QTLs were consistently detected across the three environments except for the QTLs for HD on chromosome 2A. These QTLs include known flowering gene *Ppd-A1* (*TRITD2Av1G019250*, located at approximately 36.57 Mb on the Svevo genome). Because it is known that the parental lines harbor different *Ppd-A1* alleles, we considered *Ppd-A1* to underlie these QTLs (Fig. S6). In addition, *Ppd-A1* was also detected in the QTL regions for StPS in 20A and 22AF. As TN28 harbored the photoperiod-insensitive allele, whereas LDN harbored the photoperiod-sensitive allele, as expected, the late-flowering alleles of LDN increased HD, thereby increasing StPS. On the other hand, known gene *GNI-A1*, also located on chromosome 2A (Sakuma et al. 2019), was not detected. Sequence analysis of *GNI-A1* using the two parental lines also confirmed no SNPs in *GNI-A1* (Fig. S7).

QTLs for StPS, GPSt, GPStA, and GPStC clustering on chromosome 7A were detected in 20A (Table 1; Fig. 2a). Because these QTLs were located at similar locations (QTL for StPS at 189 cM and QTLs for GPSt, GPStA, and GPStC at 187 cM by SIM), they were considered to represent a pleiotropic QTL, designated as *QYld.ku-7A*. *QYld.ku-7A* was detected for StPS, GPStA, and GPStC by both SIM and CIM methods, and for GPSt only by the SIM method. *QYld.ku-7A* was detected with LOD scores ranging from 4.99 for StPS to 13.96 for GPStA and PVE ranging from 12.10 for GPStC to 26.75 for GPStA (Table 1). The additive effects of TN28 alleles were −0.16 for GPSt, −0.25 for GPStA, and −0.15 for GPStC, whereas that for StPS was 0.90 (Table 1), indicating that TN28 alleles contribute to the increase in GPSt, GPStA, and GPStC, and the decrease in StPS. Another common QTL was detected for GPSt and GPStC on chromosome 7B by the SIM method (Table 1; Fig. 2a). To our surprise, regarding the most interesting trait GPStB in the TN28 × LDN F_2 population, only one QTL was detected on chromosome 6B in the 22AF environment by

Table 1 QTLs identified for measured traits by SIM and CIM for F_2 population across three environments

Trait	Population	QTL/gene	CHR	SIM					CIM					Additive effect[b]	PVE (%)[c]
				Closest Marker (bp)	Peak position (cM)	LOD score	CI (cM)[a]	Marker Interval (Mb)	Closest Marker (bp)	Peak Position (cM)	LOD score	CI (cM)	Marker Interval (Mb)		
HD	20A	*Ppd-A1*	2A	36211910	38	12.85	34–43	36.21–39.78	36211910	36	17.42	33–39	36.21–36.21	3.04	35.28
	22AC	*Ppd-A1*	2A	41496123	45	11.42	39–54	39.78–47.29	/					2.67	22.46
	22AF	*Ppd-A1*	2A	41848882	47	12.86	37–60	39.78–52.99	41848882	47	18.90	46–47	40.81–42.13	3.04	30.99
StPS	20A	*Ppd-A1*	2A	36211910	38	6.64	35–49	36.21–43.82	36211910	39	11.71	33–40	36.21–36.21	1.21	19.36
	20A	*QYld.ku-7A* (*WAPO1*)	7A	669537763	189	4.99	175–205	656.37–690.46	668891118	192	9.22	181–194	663.45–668.89	0.90	14.89
	22AF	*Ppd-A1*	2A	41848861	47	7.39	39–51	39.78–47.33	40813445	46	7.82	45–51	41.50–47.33	0.81	16.86
	22AF	*QStPS.ku-1B*	1B	95829345	36	4.49	19–62	25.67–413.98	/					−0.62	8.79
GPSt	20A	*QYld.ku-7A*	7A	665404737	187	5.14	178–210	658.59–690.46	/					−0.16	12.24
	20A	*QYld.ku-7B*	7B	497997630	115	4.27	106–131	443.30–566.19	/					−0.12	9.74
GPStA	20A	*QYld.ku-7A*	7A	665404737	187	9.19	181–195	663.45–668.89	665404737	187	13.96	180–191	663.45–669.54	−0.25	26.75
	22AC	*QGPStA.ku-4B*	4B	661980962	129	4.79	124–130	659.70–661.98	/					−0.13	12.45
GPStC	20A	*QYld.ku-7A*	7A	665404737	186	5.02	179–213	658.59–688.47	665404737	185	7.04	180–190	663.45–669.54	−0.15	12.10
	20A	*QYld.ku-7B*	7B	504033427	116	4.32	101–130	424.15–555.57	/					−0.12	10.08

Table 1 (continued)

Trait	Population	QTL/gene	CHR	SIM					CIM					Additive effect[b]	PVE (%)[c]
				Closest Marker (bp)	Peak position (cM)	LOD score	CI (cM)[a]	Marker Interval (Mb)	Closest Marker (bp)	Peak Position (cM)	LOD score	CI (cM)	Marker Interval (Mb)		
	22AC	*QGPStC.ku-5A*	5A	/					30821330	17	8.49	16–18	20.86–36.08	−0.13	9.86
GPStB	22AF	*QGPStB.ku-6B*	6B	528498568	92	4.44	79–109	452.29–595.99	/					−0.15	14.06

[a]QTL interval was determined by 1.8–LOD

[b]Positive and negative effects indicate alleles increasing the values of the traits from LDN and TN28, respectively

[c]Percentage of phenotypic variance explained

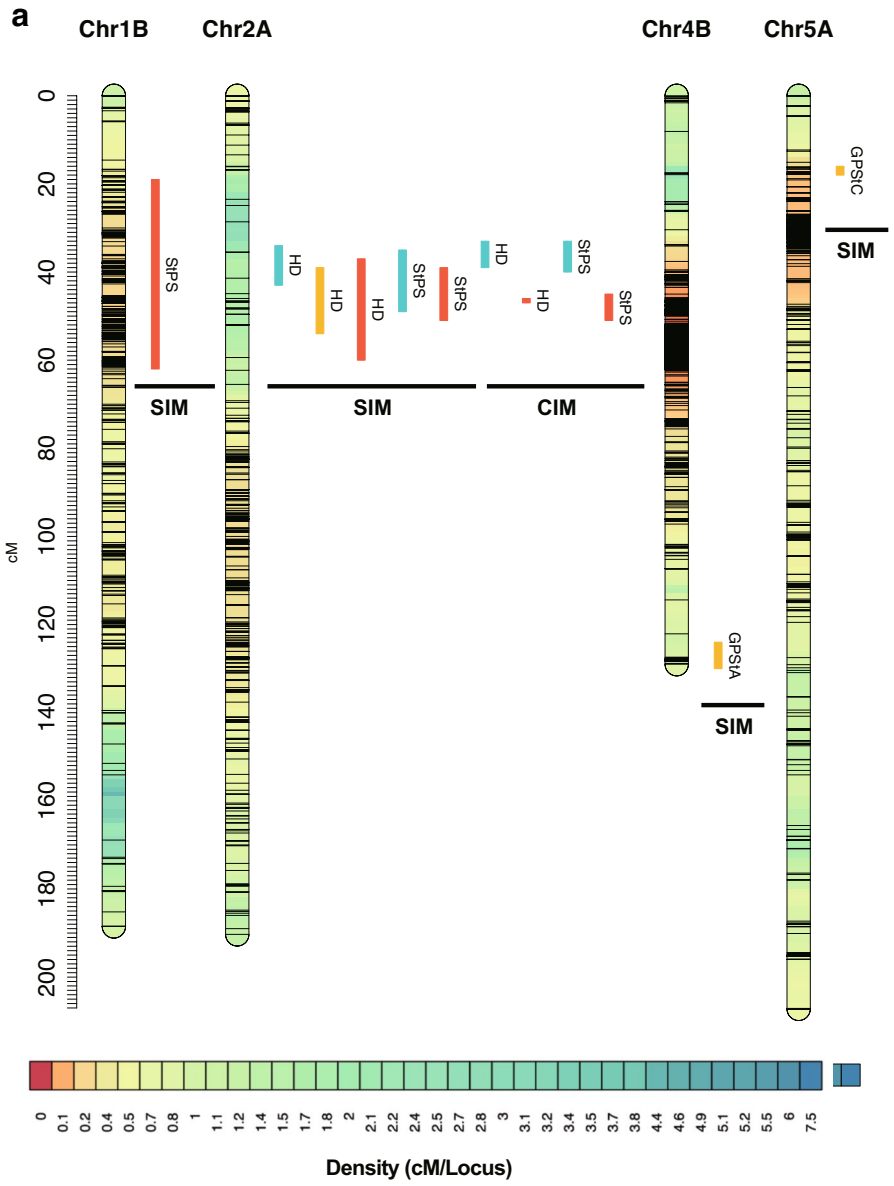


Fig. 2 Genetic linkage maps of QTLs and QTL effects of *QYld.ku-7A* on yield-related traits in F_2 population across three environments. **a** Only linkage maps with QTLs are shown. Chromosome numbers are indicated above each linkage map. Boxes on the right side of each linkage map represent the confidence intervals for QTLs. LOD peaks of QTLs are indicated by bars. Blue denotes 20A; yellow, 22AC; and orange, 22AF. SIM, simple interval mapping; CIM, composite interval mapping. **b** Effects of *QYld.ku-7A* on six yield-related traits in the F_2 population across three environments through the analysis of the InDel marker on position 663,671,083. Different lowercase letters above bars indicate significant differences among genotypes within each environment (Tukey's HSD test, $p<0.05$); bars sharing the same letter are not significantly different

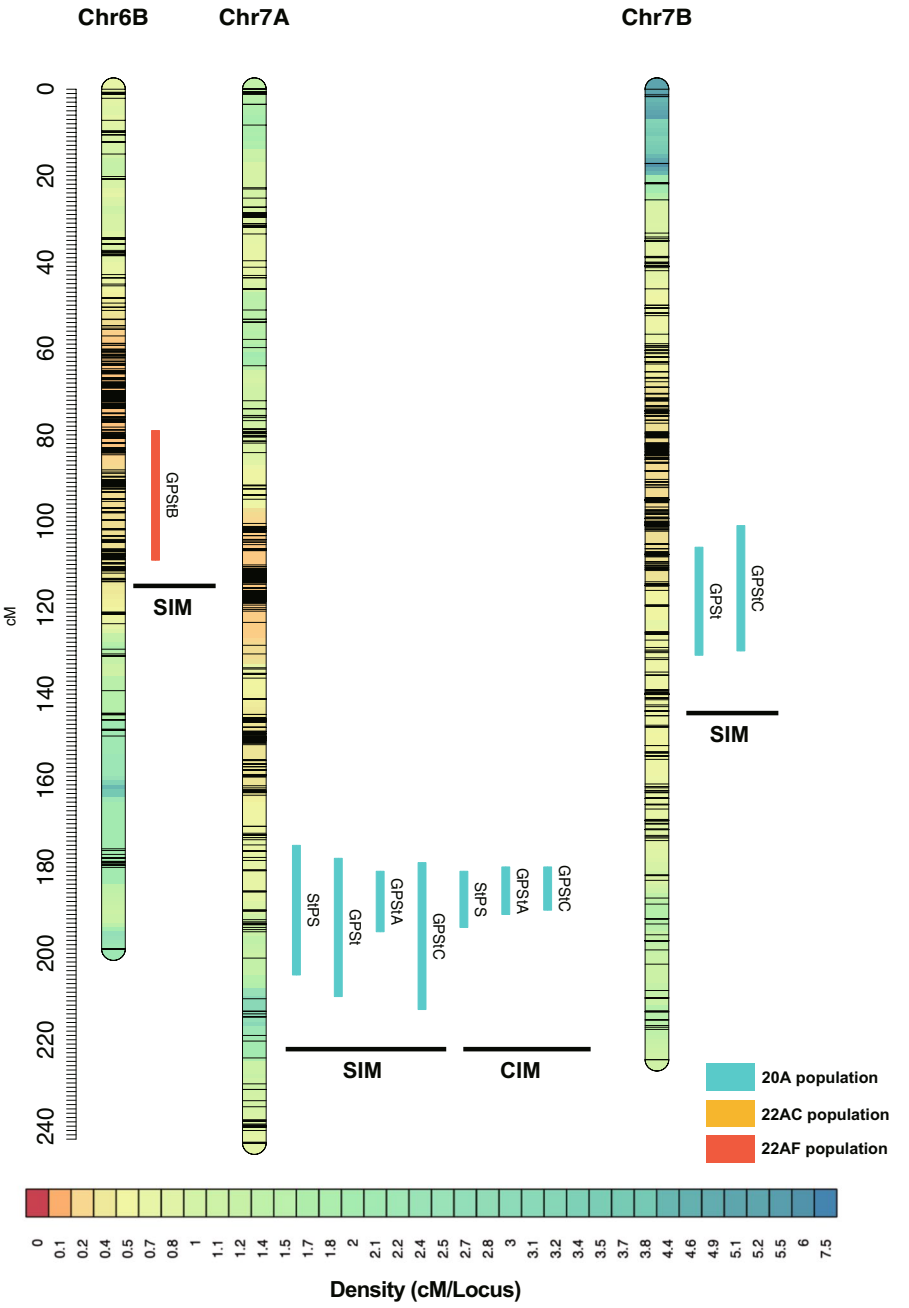


Fig. 2 (continued)

the SIM method. This QTL had an LOD score of 4.44 and exhibited a relatively high PVE value of 14.06% (Table 1). Additionally, one QTL for StPS was detected on chromosome 1B in the 22AF environment, and one QTL each for GPStA and GPStC

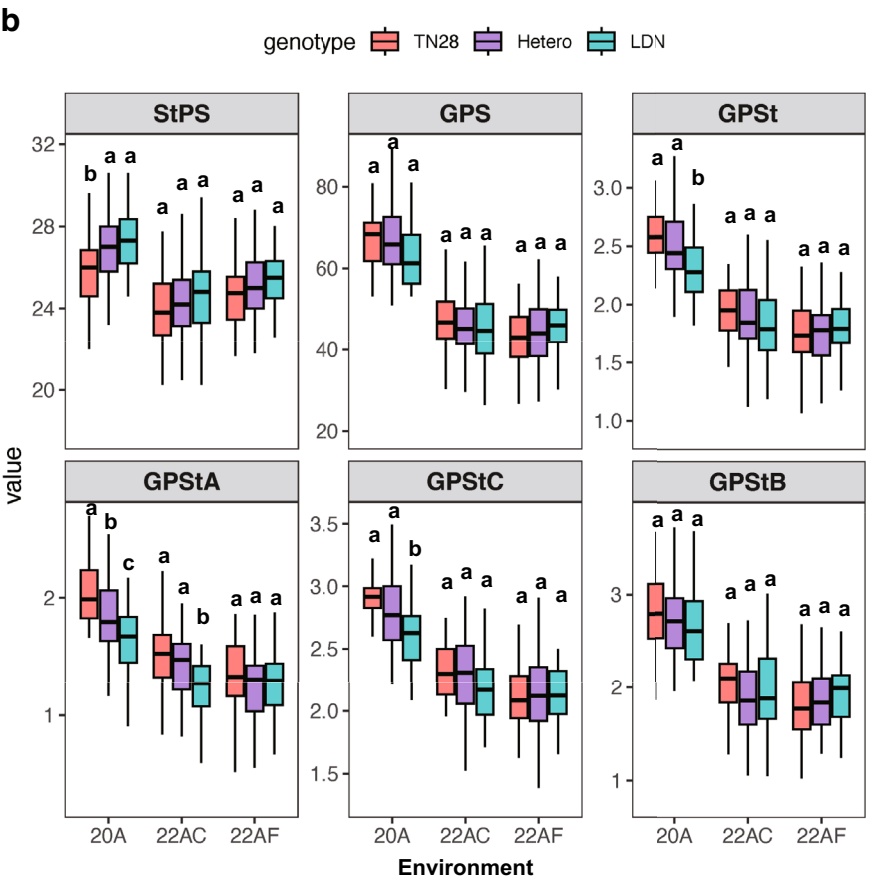


Fig. 2 (continued)

was detected on chromosomes 4B and 5A in the 22AC environment, respectively (Table 1). Taken together, we were unable to consistently detect QTLs for GPSt-related traits, the focal traits in this study, across the three environments (Fig. S8).

The effects of *QYld.ku-7A* in multiple environments

Since *QYld.ku-7A* has the most extensive effects on yield-related traits, we considered this QTL as a major QTL of interest improving grain yields. To further investigate whether the absence of detection of *QYld.ku-7A* in other two environments is caused by QTL × environment interactions or the limited power of QTL detection, a two-way anova analysis was performed using a single QTL-linked marker (Table S9). For related traits, the two-way ANOVA revealed no significant G × E interaction for StPS ($F=1.38$, $p=0.239$), whereas significant G × E interactions were detected for GPSt ($F=2.85$, $p=0.024$), GPStA ($F=3.45$, $p=0.009$), and GPStC ($F=2.80$, $p=0.026$), indicating that *QYld.ku-7A* effects on these GPSt-related traits varied across environments.

Effects of *WAPO1* on yield-related traits

WAPO1 is a major-effect gene for StPS, as reported by Muqaddasi et al. (2019) and Kuzay et al. (2019). Mapping *WAPO1* on the durum wheat reference genome revealed that *WAPO1* was positioned on approximately 667.36 Mb of chromosome 7A, which was included in the pleiotropic *QYld.ku-7A* QTL region (Table 1 and Fig. S9). Since *QYld.ku-7A* showed no QTL × environment interactions for StPS, *QYld.ku-7A* may represent a stable QTL for StPS. This stability, together with the co-localization of *WAPO1* within the *QYld.ku-7A* interval, suggested *WAPO1* as a strong candidate gene underlying *QYld.ku-7A*.

To test this hypothesis, the haplotype of *WAPO1* in two parental lines was characterized. On the basis of previous studies (Kuzay et al. 2019; Ding et al. 2022), *WAPO1* has been classified into four haplotypes (H1–H4) based on a 115-bp InDel in the promoter and a G/T SNP in the F-box region. LDN has been reported to harbor the H3 haplotype, whereas the cultivated emmer wheat accession PI 41025 harbors the H2 haplotype (Kuzay et al. 2022). To determine the TN28 haplotype, sequence alignment of *WAPO1* in TN28, LDN, and PI 41025 was performed (Fig. S10). A total of 2,375 bp of sequence around *WAPO1* was used for TN28 and LDN, comprising 720 bp upstream of the start codon and 198 bp downstream of the stop codon; for PI 41025, 2,490 bp was used, comprising 835 bp upstream of the start codon and 198 bp downstream of the stop codon. The alignment indicated that TN28 carries a 115-bp deletion in the promoter, a G allele at the F-box SNP, and an A allele at a second-exon SNP (Table S10), consistent with the H1 haplotype.

Then, the QTL effects of *QYld.ku-7A* were investigated and compared with those of *WAPO1* in the previous report. Two primer sets flanking the closest marker to *QYld.ku-7A* were developed (positions 663,671,083 and 668,299,740 on chromosome 7A; Table S4). According to the genotyping results, F_2 individuals were classified into three genotypic classes: homozygous TN28, heterozygous, and homozygous LDN. Pairwise comparison was performed using Tukey's HSD test after two-way anova analyses (Fig. 2b for the marker at position 663,671,083 and Fig. S11 for the marker at position 668,299,740; Table S10). In the 20A environment, where *QYld.ku-7A* was originally detected, the homozygous TN28 class showed significantly lower StPS than the homozygous LDN class (−1.68 spikelets, $p < 0.001$), with the heterozygous class intermediate between the two homozygous classes (Table S11 and Fig. 2b). The residual effects of *QYld.ku-7A* in the other two environments also showed the similar pattern: the homozygous TN28 class remained lower than the homozygous LDN class in 22AC (−0.99 spikelets, $p = 0.050$, marginally significant) and in 22AF (−1.12 spikelets, $p < 0.01$), mirroring the lack of a significant QTL × environment interaction noted (Table S9). These results were consistent with the previous report that H1 is associated with low StPS and H3 with high StPS (Kuzay et al. 2022), demonstrating *WAPO1* as a strong candidate gene underlying *QYld.ku-7A*.

Beyond its role in StPS, *QYld.ku-7A* was also detected as a pleiotropic QTL affecting GPSt, GPStA, and GPStC in the 20A environment. Unlike its stable effect on StPS, the effect of *QYld.ku-7A* on these GPSt-related traits showed significant QTL × environment interactions. Tukey's HSD comparisons also confirmed the magnitude and significance of QTL effects across environments. The homozygous TN28

class showed significantly higher GPSt, GPStA, and GPStC than the homozygous LDN class in 20A (all $p < 0.01$). Notably, the effects on GPStA remained significant in 22AC ($p < 0.001$). Taken together, the results indicate that *WAPO1* is a strong candidate gene underlying *QYld.ku-7A*, although other candidate genes, or genes that act in concert with *WAPO1*, may exist.

Analysis of candidate genes for *QYld.ku-7A* other than *WAPO1*

The results of QTL analysis and QTL effect confirmation indicated that *QYld.ku-7A* exhibited pleiotropic effects on both StPS and GPStA (Table 1; Fig. 2), suggesting that multiple genes underlying *QYld.ku-7A* may contribute to these traits. To identify candidate genes beyond the known gene *WAPO1* for StPS, we focused on the QTL confidence interval (CI) for GPStA, defined by the 1.8-LOD drop method and spanning 663.45–668.89 Mb (Table 1). This interval lies in the distal region of chromosome 7AL, outside the pericentromeric zone, corresponding to a segment of relatively high recombination frequency. This QTL interval contains 80 annotated high-confidence genes in the Svevo reference genome. Mutations derived from whole-genome resequencing of the two parental lines were functionally annotated with SnpEff (Table S12), which identified 30 genes carrying moderate- or high-impact variants, comprising 4 high-impact and 83 moderate-impact mutations in total. Most moderate-impact mutations were missense variants, with several mutations occurring in the same gene. On the other hand, the four high-impact mutations were located on four distinct genes: *TRITD7Av1G251730*, *TRITD7Av1G252740*, *TRITD7Av1G253400*, and *TRITD7Av1G253860*. These mutations were predicted to cause stop_gained, start_lost, frameshift_variant, and stop_lost with a concurrent splice_region_variant, respectively. Notably, known gene *WAPO1* was not classified as a high-confidence gene in durum wheat cv. Svevo; therefore, no mutation in *WAPO1* was annotated with SnpEff. Next, we investigated the putative functional roles of the four candidate genes. *TRITD7Av1G252740* encodes an rRNA 2'-O-methyltransferase, fibrillarin 2, indicating a potential role in rRNA modification. *TRITD7Av1G253860*, which encodes a haloacid dehalogenase-like hydrolase domain-containing protein 3, is associated with cellular metabolic functions. *TRITD7Av1G251730* and *TRITD7Av1G253400* encode F-box family proteins, which are typically involved in protein–protein interactions and regulatory processes. Furthermore, sequence alignment using the four genes showed that the four mutations are loss-of-function mutations in the LDN type. Because the F-box gene family is among the largest superfamilies of regulatory proteins that regulate various biological processes related to plant growth, the two genes encoding F-box proteins may be strong candidates.

Predictive ability of genomic prediction models

QTL analysis identified stable major-effect QTLs for HD and StPS but not for other yield-related traits. To determine whether this failure resulted from polygenic control (multiple genes with minor effects) or environmental variation, we applied GS, which effectively captures both major- and minor-effect alleles underlying complex traits. A marker set of 8,870 markers identified from parents and all individuals in the

three F_2 population was used to build prediction models with five statistical methods: LASSO, RR, GBLUP, RF, and ELM (Table S13). Each prediction model was trained using one F_2 population as TP and validated by correlating GEBVs with observed phenotypes in the remaining two environments as BPs (Fig. S1).

Predictive ability for HD and StPS were consistently higher than those for other yield-related traits (Table S14; Fig. 4). For HD, LASSO performed best across all scenarios, with Pearson's correlation coefficients ranging from $r=0.47$ ($p<0.001$, 22AF as TP and 22AC as BP) to $r=0.53$ ($p<0.001$, 20A as TP and 22AC as BP). For StPS, LASSO also showed stable performance, with r values ranging from 0.28 ($p<0.001$, 22AC as TP and 20A as BP) to 0.58 ($p<0.001$, 20A as TP and 22AF as BP). Notably, when 20A was used as TP and 22AF as BP, all prediction models performed well for StPS but poorly for other spike-related traits (Table S14, Fig. S12). In contrast, predictive ability for GPS and GPSt-related traits varied considerably across prediction models and scenarios. Scenarios using 22AC as TP generally outperformed those using 20A or 22AF as TP (Table S14, Fig. S12). Among the five prediction models, RR and GBLUP exhibited consistently moderate performance for all GPS and GPSt-related traits. In contrast, LASSO, RF, and ELM exhibited erratic patterns. For example, when 22AC was used as TP and 20A as BP, RR achieved moderate correlations: GPS ($r=0.25$, $p<0.01$), GPSt ($r=0.31$, $p<0.001$), GPStA ($r=0.31$, $p<0.001$), GPStC ($r=0.25$, $p<0.01$), and GPStB ($r=0.34$, $p<0.001$). Similarly, when 22AC was used as TP and 22AF as BP, RR maintained robust performance: GPS ($r=0.25$, $p<0.01$), GPSt ($r=0.18$, $p<0.01$), GPStA ($r=0.24$, $p<0.01$), GPStC ($r=0.15$, ns), and GPStB ($r=0.29$, $p<0.01$). The contrasting model performances reveal distinct genetic architectures. LASSO's superiority for HD and StPS confirms major-effect QTL control. On the other hand, RR's consistent effectiveness for GPSt-related traits—despite the absence of stable QTLs—indicates polygenic control by numerous minor-effect loci distributed across the genome (Fig. 4). These results demonstrate that GPS- and GPSt-related traits can be effectively improved through GS, even when conventional QTL mapping fails to identify significant associations. Furthermore, when predicting parental phenotypes using these GS models, TN28's predicted values were higher than LDN's for almost all GPSt-related traits data (Table S15), although only RR and LASSO for 22AC failed to predict traits. These results indicate that these prediction models accurately reflect parental genetic ability. Given that the traits were predictable by GS and that differences in parental traits were properly reflected, it was considered that TN28's GPStB and GPStC are good traits formed by the additive accumulation of multiple minor-effect genes. Given RR's stable performance, this model was selected for subsequent analyses of the effects of selection proportion on GPSt-related traits.

Genomic selection efficiency based on selection proportion

To evaluate the effects of selection proportion on breeding efficiency, we compared phenotypic performance between superior and inferior lines across selection proportions (5%–50% in increments of 5%). Within each proportion, superior and inferior groups were identified from BPs based on GEBV rankings from the RR model. We focused on GPStB as the primary target trait and evaluated selection efficiency under

various GS scenarios (Fig. S13). Superior lines showed progressively better performance as selection became more stringent across most scenarios (Table S16; Fig. 3). Mean GPStB increased from 1.97–2.82 at 50% selection to 2.11–3.03 at 5% selection. Conversely, inferior lines showed a decline in mean GPStB from 1.78–2.65 at 50% selection to 1.59–2.60 at 5% selection. The differentiation between groups intensified with increasing selection stringency. Even in scenarios with low predictive ability (using 20A as TP), where both superior and inferior lines showed declining GPStB values as the selection proportion increased, effective differentiation was still achieved because inferior lines declined more rapidly than superior lines (Table S16). The maximum difference of 0.708 GPStB ($p<0.01$) occurred at 5% selection when 22AF was TP and 22AC was BP, followed by significant differences of 0.624

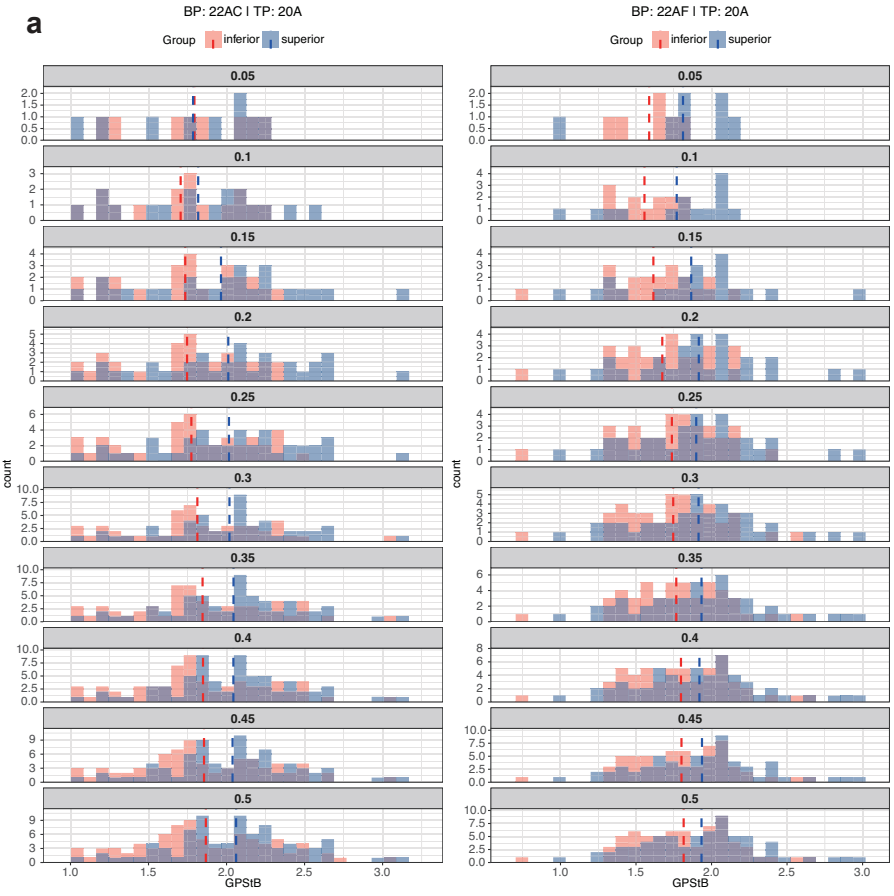


Fig. 3 Frequency distributions of GPStB for the superior and inferior groups at different selection proportions by the ridge regression model in six genomic selection scenarios. Genomic selection for GPStB using 20A as TP (**a**), 22AC as TP (**b**), and 22AF as TP (**c**). Red dashed lines indicate the mean GPStB of each environment. TP: training population. Red denotes the inferior group, and blue denotes the superior group

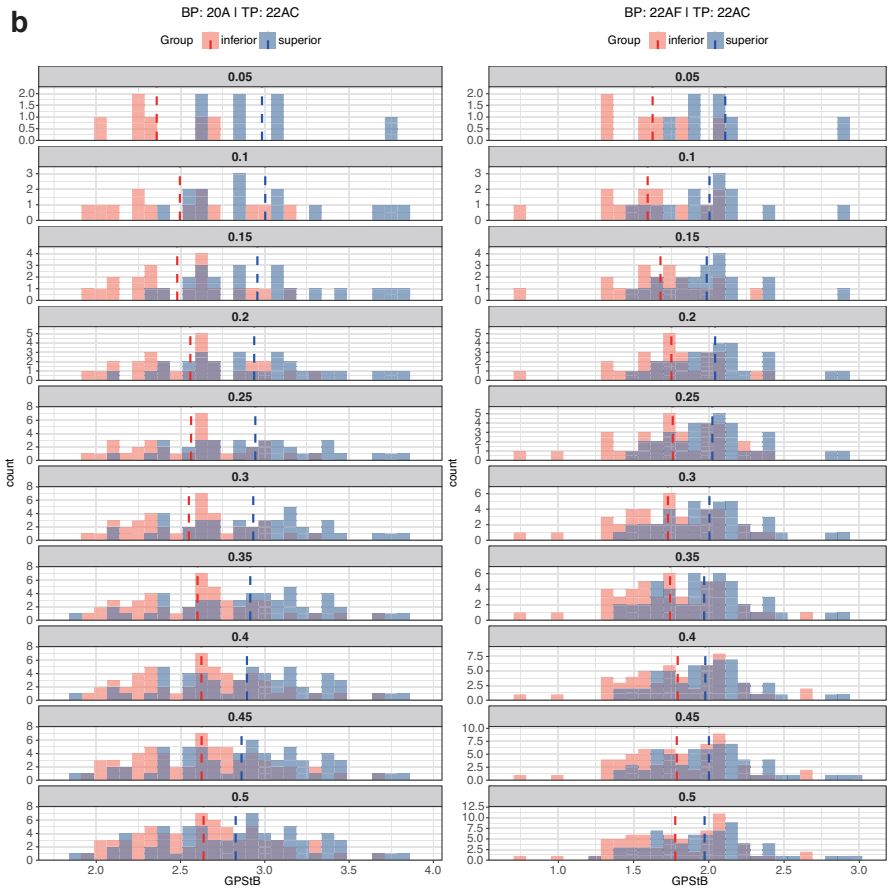


Fig. 3 (continued)

GPStB ($p<0.01$) and 0.506 GPStB ($p<0.01$) at 5% and 10% selection, respectively, when 22AC was TP and 20A was BP (Table S16). Importantly, at 20% selection proportion, RR achieved significant differentiation between superior and inferior lines across all six GS scenarios, with differences ranging from 0.261 GPStB to 0.379 GPStB (Table S16; Fig. 3). This universal effectiveness at 20% selection across all scenarios, in combination with the practical consideration of maintaining an adequate population size for breeding programs, identified 20% as the optimal selection proportion. To evaluate breeding efficiency at this selection proportion, we quantified the selection response for GPStB as the phenotypic difference between selected superior individuals and the initial BP mean. The phenotypic advantages for GPStB ranged from 5.61% (response = 0.106; ns) to 9.09% (response = 0.167; $p<0.05$) when the 22AC and 22AF environments served as TPs. In contrast, modest phenotypic advantages of 2.55% (response = 0.048; ns) to 2.67% (response = 0.041; ns) were observed when 20A was used as TP (Table S16). Overall, the progressive increase in differentiation with increasing selection stringency, coupled with the substantial phenotypic

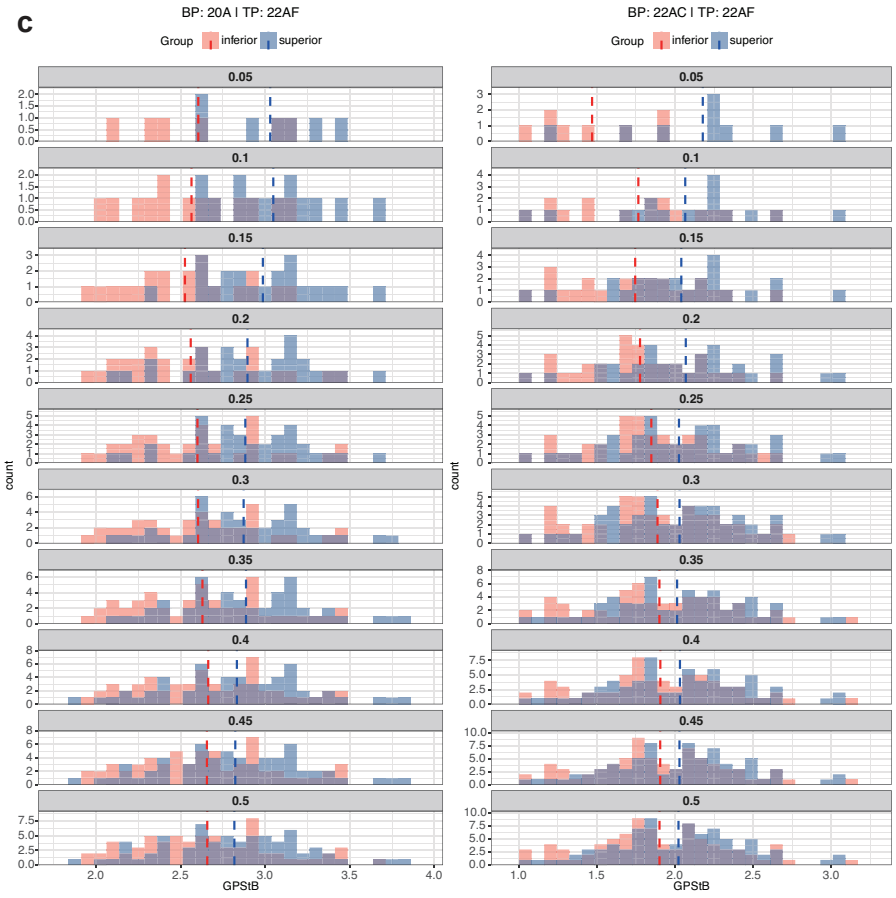


Fig. 3 (continued)

advantages achieved at 20% selection proportion across all GS scenarios, confirms that GS effectively captures genetic variation underlying GPStB. This pattern is characteristic of polygenic traits controlled by multiple minor-effect loci rather than a few major-effect genes, corroborating our inference from the RR prediction performance.

Correlated response in GPS at the optimal selection proportion

Because this single-trait GS model focuses on GPStB, we further evaluated the correlated response in GPS, the primary trait determining final yield, to assess potential genetic trade-offs when selecting for GPStB at 20% selection proportion (Fig. S14; Table S17). Most scenarios showed favorable correlated responses with phenotypic advantages of 1.70%–7.00% in GPS. When 20A served as BP, superior lines showed modest, non-significant improvements of 1.59 GPS (2.40%) and 1.20 GPS (1.80%) with 22AC and 22AF as TPs. When 22AC served as BP, positive responses of 0.80 GPS (1.70%) and 1.85 GPS (4.00%) were observed with 20A and 22AF as

TPs. However, one unfavorable trade-off occurred when 22AF was BP with 20A as TP, showing −1.25 GPS (−2.80%). The most favorable outcome occurred when 22AC was TP and 22AF was BP, yielding a significant increase of 3.08 GPS (7.00%, $p < 0.05$). Taken together, these results demonstrate that GS using the RR prediction model at 20% selection proportion effectively identifies superior individuals for the secondary trait GPStB while maintaining favorable correlated responses for the primary trait GPS, providing a practical strategy for simultaneously improving grain quality and yield in wheat breeding.

Discussion

Improving grain yield is the main target in wheat breeding. However, the task is challenging because of the complexity of grain yield. In this study, two genomic analysis approaches were applied to evaluate grain yield-related traits in TN28, a pyramidale wheat accession. Currently, TN28 is not cultivated; rather, it serves as a genetic resource for improving wheat yield. The first approach, QTL analysis, identified stable QTLs for HD and StPS that overlap with known genes, but failed to detect stable QTLs for GPSt-related traits. The second approach, GS, effectively selected superior lines with higher GPSt-related traits, even though the data were obtained under different cultivation conditions. These results suggest that the pyramidale wheat may harbor multiple minor yield component genes, and that GS holds significant potential for selecting yield-related traits controlled by these minor-effect genes.

Wheat spikes are characterized by a lanceolate shape, with the central spikelets producing the most and largest grains, and spikelet size gradually decreases toward the apex and the base. This is due to the florets on apical spikelets having insufficient development time and those on basal spikelets being underdeveloped (Backhaus et al. 2022, 2023). Based on the Waddington scale (Waddington et al. 1983), Waddington stage 5.5, occurring 20 days before flowering, is considered the viability threshold. In this context, the reduction in grain number in the most apical and most basal spikelets is likely due to the florets failing to pass this threshold. Thus, although previous studies have indicated that the genetic mechanisms governing grain setting vary across spike sections, there is inconsistency in how the spike should be divided for genetic analysis. In most studies, researchers have sampled only representative spikelets from each section—for example, selecting three specific spikelets each from the apical, central, and basal sections of the spike. In contrast, Mizuno et al. (2021) analyzed grain number per spikelet by investigating every spikelet on the spike and partitioning them into three sections (apical, central, and basal), thereby evaluating grain number without being affected by variations in spikelet number. This comprehensive approach yielded more accurate regional measurements than limited sampling. Following this approach, we also divided the entire spike into three sections by surveying all spikelets for genetic analysis. As a result, section-specific QTLs were detected. These section-specific QTLs provide genetic evidence that distinct mechanisms regulate grain setting in different spike sections and underscore the importance of regional genetic analysis in dissecting the genetic architecture of grain number traits.

QTL studies utilize differences in phenotype and genotype to identify genomic regions associated with a phenotype of interest. To better capture phenotypic variation among F_2 individuals, five spikes were randomly sampled per plant. However, in wheat, spike fertility differs between the main stem and tiller spikes: the main stem tends to be relatively stable, whereas tiller spikes are more susceptible to environmental factors such as drought (Xu et al. 2015; Lin et al. 2020). Because the spikes sampled here were not recorded as main stem or tiller in origin, this approach may have introduced within-plant variation unrelated to genotype, confounding the differences observed among individuals. This could reduce the precision and power of QTL detection in this study. Construction of RILs that allow genetic fixation and biological replication, along with standardization of the sampling strategy to measure only the main spike, would help minimize this source of variation. Nevertheless, the fact that phenotypic differences between the two parental lines were consistently observed under all three environmental conditions, and that genomic selection allowed for at least some prediction of the traits, suggests that this study was able to capture genetic effects that transcended these potential sources of noise, even if not perfectly.

The availability of the durum wheat reference genome facilitated comparison of detected QTLs with previously reported QTLs/genes. In this study, QTL analysis of yield-related traits was performed using a genetic map constructed from SNP markers whose physical positions are indicated on the durum wheat reference genome. Thus, the physical positions of QTLs on the durum wheat reference genome could be readily retrieved and considered for potential co-location with known genes and QTLs we detected. From the results of QTL analysis in this study, QTLs were detected on chromosomes 1B, 2A, 4B, 5A, 6B, 7A, and 7B. QTLs on chromosome 2A for HD and StPS corresponded to known gene *Ppd-A1*, as the parental lines harbored different *Ppd-A1* alleles. *WAPO1* was the gene responsible for QTLs on chromosome 7A for StPS, as described before. To identify candidate genes for other QTLs on chromosomes 1B, 4B, 5A, 6B, and 7B, their physical positions were used to perform a comparison analysis with known genes for yield-related traits projected on the durum wheat reference genome. Three well-known genes responsible for spike morphological traits are *Q*, *Compactum* (C), and *Sphaerococcum* (*S*), which have been identified on chromosomes 5AL, 2DL, and 3DS, respectively (Johnson et al. 2008; Cui et al. 2012; Faris et al. 2014). All three genes give rise to a compact spike, whereas the *Q* gene, a key domestication gene, exhibits pleiotropic effects on yield-related traits, including HD and GPSt. However, the QTL detected in this study was on the short arm of chromosome 5A, whereas *Q* was on the long arm. The recently cloned gene *TaCol-B5*, which is associated with StPS, is located on chromosome 7BL (Zhang et al. 2022). In contrast, we found that *TaCol-B5* was −15 Mb away from the QTL detected on chromosome 7B. Additionally, *TEOSINTE BRANCHED-D1* (*TB-D1*), which regulates spikelet number, and the essential "Green revolution" gene *Rht-B1*, which reduces plant height and also significantly affects yield-related traits, have been identified on chromosome 4B (Dixon et al. 2018; Guan et al. 2018). However, they are both located on the short arm of chromosome 4B, whereas the QTLs we detected were located on the long arm. To our knowledge, no cloned genes for spike-related traits have been identified on chromosomes 1B and 6B. On the other hand, many QTLs for spike-related traits have been reported. Thus, we conducted a rough comparison of

QTLs detected in this study with previously reported yield-related QTLs in tetraploid wheat QTLome (Maccaferri et al. 2019) and with the work of Kiros et al. (2024), which summarizes QTLs for StPS and GPSt through December 2023. Many previously reported QTLs overlapped with the QTL regions identified in this study, but few were for the same trait. For example, numerous QTLs have been reported to co-locate with the QTL for GPStB on chromosome 6B, whereas only the QTL reported by Roncallo et al. (2017) is also for GPSt. Similarly, the QTL for GPStC on chromosome 5A may correspond to the QTLs for GPSt reported by Giunta et al. (2018). The QTL for GPStA on chromosome 4B may correspond to the QTL reported by Maccaferri et al. (2019). The large span of QTL for StPS on chromosome 1B overlapped with the QTLs for StPS reported by Faris et al. (2014) and Roncallo et al. (2017) and the QTL for spike fertility reported by Maccaferri et al. (2019). Although few previously mapped QTLs overlapped with the QTL regions in this study, this overlap might be due to the use of different mapping populations from crosses between different parents. In this study, we found that overlapping QTL regions may result from genetic diversity of the parental lines at different loci. Although these QTLs were co-located in overlapping regions, their effects were not sufficiently large to be stably detected and used in a MAS program for wheat breeding.

The comparative results of QTL mapping and GS provide complementary evidence for understanding the genetic architecture of yield-related traits in TN28, a pyramidale wheat accession. QTL stability across various environments was related to the prediction performance of LASSO and RR. For HD and StPS, QTL mapping detected stable QTLs across different environments, indicating major-effect gene control of these traits. Consistent with this genetic architecture, GS using LASSO, which performs variable selection by retaining major-effect loci while shrinking minor-effect markers to zero, achieved high predictive ability for these traits (Fig. 4). For example, a stable QTL corresponding to *Ppd-A1* was detected for StPS in both 20A and 22AF, with LASSO achieving reciprocal predictive ability of 0.58 and 0.53 ($p < 0.001$) between these environments (Table S14). An intermediate pattern was observed for GPStA. A QTL, *QYld.ku-7A*, was detected in 20A and its corresponding marker effect remained significant when tested in 22AC (Table 1; Fig. 2b). Thus, this intermediate level of QTL stability corresponded to intermediate LASSO performance, with correlations of 0.30 and 0.42 between 20 and 22AC (Table S14). In contrast, GPS and the GPSt-related traits other than GPStA exhibited a third pattern. QTLs identified for these traits are environment-specific and their corresponding marker effects also did not reach significance when tested in other environments, suggesting the absence of major-effect loci with consistent effects. Consequently, LASSO performed poorly for these traits, whereas RR, which assumes uniform shrinkage across all markers and effectively captures the cumulative effects of numerous minor-effect loci, exhibited consistent moderate predictive ability across all prediction scenarios (Table S14). Taken together, the concordance between QTL stability and GS model performance suggests that yield-related traits in TN28 differ substantially in their underlying genetic architecture. Traits associated with stable QTLs across environments were more effectively predicted by LASSO, reflecting the contribution of major-effect loci, whereas traits lacking stable QTLs were generally better captured by RR, consistent with the cumulative effects of numerous small-effect loci.

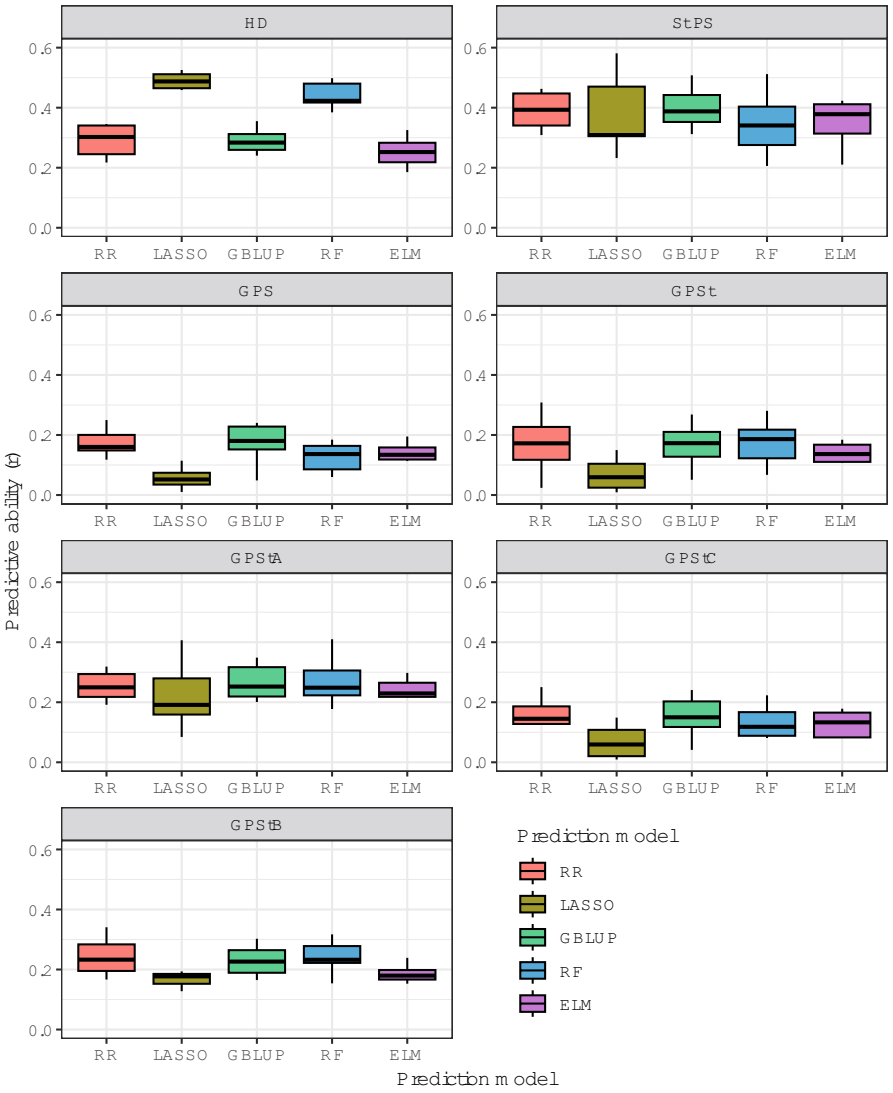


Fig. 4 Predictive ability of five prediction models for measured yield-related traits across all genomic selection scenarios. Measured traits included heading date (HD), spikelet number per spike (StPS), grain number per spike (GPS), grain number per spikelet (GPSt), GPSt at the apical section of the spike (GPStA), GPSt at the central section of the spike (GPStC), and GPSt at the basal section of the spike (GPStB). The five prediction models include ridge regression (RR), LASSO, GBLUP, random forest (RF), and extreme learning machine (ELM). In each boxplot, the solid horizontal line indicates the median value, and the upper and lower edges of the box represent the first and third quartiles, respectively

Recently, multi-trait and multi-environment (MTME) models have been proposed to improve GS by accounting for both limited population size and G × E interactions. MTME models leverage genetic correlations among traits and environments to increase effective TP size (Merrick et al. 2022). Gill et al. (2021) demonstrated that MTME models outperformed single-trait models across 10 site-year environ-

ments. By jointly modeling population-by-year combinations and correlated yield-related traits, MTME approaches may improve predictive ability while accounting for G × E interactions. This approach holds promise for polygenic traits like GPSt-related traits, where capturing distributed genetic effects across contexts is essential. This study collected data from three environments over two years, thereby limiting the applicability of such models. Moving forward, it is crucial to further enhance GS predictive ability by using genetically fixed materials, such as RILs, and models that account for these G × E interactions.

Conclusion

We characterized the genetic factors underlying the high yield potential of TN28. Our analysis revealed that the increased GPSt in TN28 is localized to the middle and basal sections of the spike. QTL mapping detected no stable loci for GPSt-related traits across environments, whereas GS showed promise for identifying superior individuals with higher yield-related traits. Together, these results are consistent with a polygenic basis for TN28's high-yield phenotype and supports the feasibility of GS in early-generation segregating material such as F_2 populations. From a breeding perspective, however, selection is typically implemented at more advanced, fixed generations. Future studies should therefore extend genomic prediction to such generations to enhance its practical utility in wheat breeding.

Abbreviations

ANOVA	Analysis of variance
BP	Breeding population
CI	Confidence interval
CIM	Composite interval mapping
EC	Electrical conductivity
ELM	Extreme learning machine
GBLUP	Genomic best linear unbiased predictor
GEBVs	Genomic estimated breeding values
GNI1	Grain Number Increase 1
GPS	Grain number per spike
GPSt	Grain number per spikelet
GPStA	Grain number per spikelet at the apical section of the spike
GPStB	Grain number per spikelet at the basal section of the spike
GPStC	Grain number per spikelet at the central section of the spike
GRM	Genomic relationship matrix
GS	Genomic selection
GWAS	Genome-wide association studies
HD	Heading date
InDel	Insertion-Deletion
LASSO	Least absolute shrinkage and selection operator
LOD	Logarithm of the odds
MAS	Marker-assisted selection

MIG-seq	Multiplexed inter-simple sequence repeats genotyping by sequencing
PRR	Pseudo-response regulator
PVE	Phenotypic variance explained
QTL	Quantitative trait locus
RF	Random forest
RKHS	Reproducing kernel Hilbert space
RR	Ridge regression
SIM	Simple interval mapping
SNP	Single-nucleotide polymorphism
StPS	Spikelet number per spike
TP	Training population
VCF	Variant call format
WAPO1	WHEAT ORTHOLOG OF APO1

Supplementary Information The online version contains supplementary material available at https://doi.org/10.1007/s11032-026-01728-8.

Acknowledgements A tetraploid wheat cultivar, "Langdon" was provided by the National BioResource Project–Wheat with support in part from the National BioResource Project of MEXT, Japan. This work was supported by a Grant-in-Aid for Early-Career Scientists (23K13929) from the Japan Society for the Promotion of Science. We deeply thank a team to cultivate field-crops in Experimental Farm of Kyoto University (chief, Mr. Hisashi Kagata) for supporting cultivation of wheat plants.

Author contributions Kazusa Nishimura, Takanori Yoshikawa, Ryohei Nakano, and Tetsuya Nakazaki conceived and designed the study. Kyoka Nagasaka, Takahiro Maki, Ko Motoki, and Yu Kinoshita contributed to the discussion of the research design and the interpretation of results. Tiantian Chen performed wheat cultivation and phenotypic measurements with support from Kazuki Murata, Kazusa Nishimura, Yu Iwahashi, and Hiromo Inoue. Tiantian Chen, Ryohei Nakano, and Kazusa Nishimura performed the genotyping experiments. Tiantian Chen performed bioinformatics, QTL analysis, and genomic selection under the supervision of Kazusa Nishimura. Tiantian Chen wrote the original draft, and all authors contributed to the revision. All authors have read and approved the final manuscript.

Funding This work was supported by JSPS KAKENHI Grant Number JP23K13929.

Data availability The raw sequencing data generated in this study have been deposited in the DDBJ Sequence Read Archive (DRA) and are available under BioProject accession numbers PRJDB40418 and PRJDB40154.

Declarations

Competing interests The authors declare no competing interests.

Open Access This article is licensed under a Creative Commons Attribution-NonCommercial-NoDerivatives 4.0 International License, which permits any non-commercial use, sharing, distribution and reproduction in any medium or format, as long as you give appropriate credit to the original author(s) and the source, provide a link to the Creative Commons licence, and indicate if you modified the licensed material. You do not have permission under this licence to share adapted material derived from this article or parts of it. The images or other third party material in this article are included in the article's Creative Commons licence, unless indicated otherwise in a credit line to the material. If material is not included in the article's Creative Commons licence and your intended use is not permitted by statutory regulation or exceeds the permitted use, you will need to obtain permission directly from the copyright holder. To view a copy of this licence, visit http://creativecommons.org/licenses/by-nc-nd/4.0/.

References

Anilkumar C, Sunitha NC, Harikrishna, et al (2022) Advances in integrated genomic selection for rapid genetic gain in crop improvement: a review. Planta 256. https://doi.org/10.1007/s00425-022-03996-y

Backhaus AE, Lister A, Tomkins M et al (2022) High expression of the MADS-box gene VRT2 increases the number of rudimentary basal spikelets in wheat. Plant Physiol 189:1536–1552. https://doi.org/10.1093/plphys/kiac156

Backhaus AE, Griffiths C, Vergara-Cruces A et al (2023) Delayed development of basal spikelets in wheat explains their increased floret abortion and rudimentary nature. J Exp Bot 74:5088–5103. https://doi.org/10.1093/jxb/erad233

Beales J, Turner A, Griffiths S et al (2007) A Pseudo-Response Regulator is misexpressed in the photoperiod insensitive Ppd-D1a mutant of wheat (*Triticum aestivum* L.). Theor Appl Genet 115:721–733. https://doi.org/10.1007/s00122-007-0603-4

Bernardo R (2008) Molecular markers and selection for complex traits in plants: learning from the last 20 years. Crop Sci 48:1649–1664. https://doi.org/10.2135/cropsci2008.03.0131

Bernardo R (2014) Genomewide selection when major genes are known. Crop Sci 54:68–75. https://doi.org/10.2135/cropsci2013.05.0315

Bernardo R (2020) Reinventing quantitative genetics for plant breeding: something old, something new, something borrowed, something BLUE. Heredity (Edinb) 125:375–385. https://doi.org/10.1038/s41437-020-0312-1

Boden SA, Cavanagh C, Cullis BR et al (2015) *Ppd-1* is a key regulator of inflorescence architecture and paired spikelet development in wheat. Nat Plants. https://doi.org/10.1038/nplants.2014.16

Boden SA, McIntosh RA, Uauy C et al (2023) Updated guidelines for gene nomenclature in wheat. Theor Appl Genet. https://doi.org/10.1007/s00122-023-04253-w

Broman KW, Wu H, Sen Ś, Churchill GA (2003) R/qtl: QTL mapping in experimental crosses. Bioinformatics 19:889–890. https://doi.org/10.1093/bioinformatics/btg112

Chen D, Wu X, Wu K et al (2017) Novel and favorable genomic regions for spike related traits in a wheat germplasm Pubing 3504 with high grain number per spike under varying environments. J Integr Agric 16:2386–2401. https://doi.org/10.1016/S2095-3119(17)61711-8

Chen S, Zhou Y, Chen Y, Gu J (2018) Fastp: an ultra-fast all-in-one FASTQ preprocessor. Bioinformatics 34:i884–i890. https://doi.org/10.1093/bioinformatics/bty560

Churchill GA, Doerge RW (1994) Empirical threshold values for quantitative trait mapping. Genetics 138:963–971. https://doi.org/10.1093/genetics/138.3.963

Cingolani P, Platts A, Wang LL et al (2012) A program for annotating and predicting the effects of single nucleotide polymorphisms, SnpEff: SNPs in the genome of *Drosophila melanogaster* strain w1118; iso-2; iso-3. Fly (Austin) 6:80–92. https://doi.org/10.4161/fly.19695

Cui F, Ding A, Li J et al (2012) QTL detection of seven spike-related traits and their genetic correlations in wheat using two related RIL populations. Euphytica 186:177–192. https://doi.org/10.1007/s10681-011-0550-7

Danecek P, Auton A, Abecasis G et al (2011) The variant call format and VCFtools. Bioinformatics 27:2156–2158. https://doi.org/10.1093/bioinformatics/btr330

Ding P, Mo Z, Tang H et al (2022) A major and stable QTL for wheat spikelet number per spike validated in different genetic backgrounds. J Integr Agric 21:1551–1562. https://doi.org/10.1016/S2095-3119(20)63602-4

Dixon LE, Greenwood JR, Bencivenga S et al (2018) TEOSINTE BRANCHED1 regulates inflorescence architecture and development in bread wheat (*Triticum aestivum*). Plant Cell 30:563–581. https://doi.org/10.1105/tpc.17.00961

FAO, IFAD, UNICEF, WFP, WHO (2023) The state of food security and nutrition in the world 2023. Urbanization, agrifood systems transformation and healthy diets across the rural–urban continuum. FAO, Rome. https://doi.org/10.4060/cc3017en

Faris JD, Zhang Q, Chao S et al (2014) Analysis of agronomic and domestication traits in a durum × cultivated emmer wheat population using a high-density single nucleotide polymorphism-based linkage map. Theor Appl Genet 127:2333–2348. https://doi.org/10.1007/s00122-014-2380-1

Friedman J, Hastie T, Tibshirani R (2010) Regularization paths for generalized linear models via coordinate descent. J Stat Softw 33:1–22. https://doi.org/10.18637/jss.v033.i01

Gill HS, Halder J, Zhang J, et al (2021) Multi-Trait Multi-Environment Genomic Prediction of Agronomic Traits in Advanced Breeding Lines of Winter Wheat. Front Plant Sci 12. https://doi.org/10.3389/fpls.2021.709545

Giunta F, De Vita P, Mastrangelo AM, et al (2018) Environmental and genetic variation for yield-related traits of durum wheat as affected by development. Front Plant Sci 9. https://doi.org/10.3389/fpls.2018.00008

Guan P, Lu L, Jia L et al (2018) Global QTL analysis identifies genomic regions on chromosomes 4A and 4B harboring stable loci for yield-related traits across different environments in wheat (*Triticum aestivum* L.). Front Plant Sci 9:529. https://doi.org/10.3389/fpls.2018.00529

Guo Z, Song Y, Zhou R et al (2010) Discovery, evaluation and distribution of haplotypes of the wheat Ppd-D1 gene. New Phytol 185:841–851. https://doi.org/10.1111/j.1469-8137.2009.03099.x

Haley CS, Knott SA (1992) A simple regression method for mapping quantitative trait loci in line crosses using flanking markers. Heredity (Edinb) 69:315–324. https://doi.org/10.1038/hdy.1992.131

Hasan SS, Zhen L, Miah MG, et al (2020) Impact of land use change on ecosystem services: A review. Environ Dev 34. https://doi.org/10.1016/j.envdev.2020.100527

Huang GB, Zhu QY, Siew CK (2006) Extreme learning machine: theory and applications. Neurocomputing 70:489–501. https://doi.org/10.1016/j.neucom.2005.12.126

Johnson EB, Nalam VJ, Zemetra RS, et al (2008) Mapping the compactum locus in wheat (*Triticum aestivum* L.) and its relationship to other spike morphology genes of the Triticeae. Euphytica 163:193–201. https://doi.org/10.1007/s10681-007-9628-1

Kiros AY, Mica E, Battaglia R, et al (2024) Independent genetic factors control floret number and spikelet number in Triticum turgidum ssp. Front Plant Sci 15. https://doi.org/10.3389/fpls.2024.1390401

Kuzay S, Xu Y, Zhang J et al (2019) Identification of a candidate gene for a QTL for spikelet number per spike on wheat chromosome arm 7AL by high-resolution genetic mapping. Theor Appl Genet 132:2689–2705. https://doi.org/10.1007/s00122-019-03382-5

Kuzay S, Lin H, Li C et al (2022) WAPO-A1 is the causal gene of the 7AL QTL for spikelet number per spike in wheat. PLoS Genet. https://doi.org/10.1371/journal.pgen.1009747

Li H, Handsaker B, Wysoker A et al (2009) The sequence alignment/map format and SAMtools. Bioinformatics 25:2078–2079. https://doi.org/10.1093/bioinformatics/btp352

Lin X, Li P, Shang Y et al (2020) Spike formation and seed setting of the main stem and tillers under post-jointing drought in winter wheat. J Agron Crop Sci 206:694–710. https://doi.org/10.1111/jac.12432

Lin Y, Jiang X, Hu H et al (2021) QTL mapping for grain number per spikelet in wheat using a high-density genetic map. Crop J 9:1108–1114. https://doi.org/10.1016/j.cj.2020.12.006

Liu X, Zhu P, Liu S et al (2024) Global cropland expansion enhances cropping potential and reduces its inequality among countries. Earth Syst Dynam 15:817–828. https://doi.org/10.5194/esd-15-817-2024

Maccaferri M, Harris NS, Twardziok SO et al (2019) Durum wheat genome highlights past domestication signatures and future improvement targets. Nat Genet 51:885–895. https://doi.org/10.1038/s41588-019-0381-3

Manichaikul A, Dupuis J, Sen Ś, Broman KW (2006) Poor performance of bootstrap confidence intervals for the location of a quantitative trait locus. Genetics 174:481–489. https://doi.org/10.1534/genetics.106.061549

Matsuoka Y, Mori N (2020) Reproductive and genetic roles of the maternal progenitor in the origin of common wheat (*Triticum aestivum* L.). Ecol Evol 10:13926–13937. https://doi.org/10.1002/ece3.6985

Merrick LF, Herr AW, Sandhu KS et al (2022) Optimizing plant breeding programs for genomic selection. Agronomy 12:714. https://doi.org/10.3390/agronomy12030714

Meuwissen TH, Hayes BJ, Goddard M (2001) Prediction of total genetic value using genome-wide dense marker maps. Genetics 157(4):1819–1829. https://doi.org/10.1093/genetics/157.4.1819

Mizuno N, Ishikawa G, Kojima H et al (2021) Genetic mechanisms determining grain number distribution along the spike and their effect on yield components in wheat. Mol Breed. https://doi.org/10.1007/s11032-021-01255-8

Muqaddasi QH, Brassac J, Koppolu R et al (2019) TaAPO-A1, an ortholog of rice ABERRANT PANICLE ORGANIZATION 1, is associated with total spikelet number per spike in elite European hexaploid winter wheat (*Triticum aestivum* L.) varieties. Sci Rep. https://doi.org/10.1038/s41598-019-50331-9

Nguyen AT, Nishijima R, Kajimura T et al (2015) Quantitative trait locus analysis for flowering-related traits using two F2 populations derived from crosses between Japanese common wheat cultivars and synthetic hexaploids. Genes Genet Syst 90:89–98. https://doi.org/10.1266/ggs.90.89

Nishimura K, Moriyama R, Katsura K et al (2018) The early flowering trait of an emmer wheat accession (*Triticum turgidum* L. ssp. *dicoccum*) is associated with the cis-element of the Vrn-A3 locus. Theor Appl Genet 131:2037–2053. https://doi.org/10.1007/s00122-018-3131-5

Nishimura K, Kokaji H, Motoki K et al (2024) Degenerate oligonucleotide primer MIG-seq: an effective PCR-based method for high-throughput genotyping. Plant J 118:2296–2317. https://doi.org/10.1111/tpj.16708

Nishimura K, Motoki K, Yamazaki A et al (2022) MIG-seq is an effective method for high-throughput genotyping in wheat (*Triticum* spp.). DNA Res. https://doi.org/10.1093/dnares/dsac011

Ochagavía H, Prieto P, Savin R et al (2018) Dynamics of leaf and spikelet primordia initiation in wheat as affected by Ppd-1a alleles under field conditions. J Exp Bot 69:2621–2631. https://doi.org/10.1093/jxb/ery104

Ogbonnaya FC, Abdalla O, Mujeeb-Kazi A et al (2013) Synthetic hexaploids: harnessing species of the primary gene pool for wheat improvement. Plant breeding reviews. John Wiley & Sons, Inc., Hoboken, NJ, USA, pp 35–122

Pérez P, De Los Campos G (2014) Genome-wide regression and prediction with the BGLR statistical package. Genetics 198:483–495. https://doi.org/10.1534/genetics.114.164442

Potapov P, Turubanova S, Hansen MC et al (2022) Global maps of cropland extent and change show accelerated cropland expansion in the twenty-first century. Nat Food 3:19–28. https://doi.org/10.1038/s43016-021-00429-z

Prieto P, Ochagavía H, Savin R, Griffiths S, Slafer GA (2018) Dynamics of floret initiation/death determining spike fertility in wheat as affected by Ppd genes under field conditions. J Exp Bot 69:2633–2645. https://doi.org/10.1093/jxb/ery105

Rastas P (2017) Lep-MAP3: robust linkage mapping even for low-coverage whole genome sequencing data. Bioinformatics 33:3726–3732. https://doi.org/10.1093/bioinformatics/btx494

Robinson JT, Thorvaldsdóttir H, Wenger AM et al (2017) Variant review with the Integrative Genomics Viewer. Cancer Res 77:e31–e34. https://doi.org/10.1158/0008-5472.CAN-17-0337

Roncallo PF, Akkiraju PC, Cervigni GL, Echenique VC (2017) QTL mapping and analysis of epistatic interactions for grain yield and yield-related traits in *Triticum turgidum* L. var. durum. Euphytica. https://doi.org/10.1007/s10681-017-2058-2

Sakuma S, Golan G, Guo Z et al (2019) Unleashing floret fertility in wheat through the mutation of a homeobox gene. Proc Natl Acad Sci USA 116:5182–5187. https://doi.org/10.1073/pnas.1815465116

Shitsukawa N, Kinjo H, Takumi S, Murai K (2009) Heterochronic development of the floret meristem determines grain number per spikelet in diploid, tetraploid and hexaploid wheats. Ann Bot 104:243–251. https://doi.org/10.1093/aob/mcp129

Tay JK, Narasimhan B, Hastie T (2023) Elastic Net Regularization Paths for All Generalized Linear Models. J Stat Softw 106. https://doi.org/10.18637/jss.v106.i01

Waddington SR, Cartwright PM, Wall PC (1983) A quantitative scale of spike initial and pistil development in barley and wheat. Ann Bot 51:119–130. https://doi.org/10.1093/oxfordjournals.aob.a086434

Worland AJ (1996) The influence of flowering time genes on environmental adaptability in European wheats. Euphytica 89:49–57. https://doi.org/10.1007/BF00015718

Wright MN, Ziegler A (2017) Ranger: A fast implementation of random forests for high dimensional data in C++ and R. J Stat Softw 77. https://doi.org/10.18637/jss.v077.i01

Xu S (2003) Theoretical basis of the Beavis effect. Genetics 165:2259–2268. https://doi.org/10.1093/genetics/165.4.2259

Xu Y, Crouch JH (2008) Marker-assisted selection in plant breeding: from publications to practice. Crop Sci 48:391–407. https://doi.org/10.2135/cropsci2007.04.0191

Xu H, Cai T, Wang Z, He M (2015) Physiological basis for the differences of productive capacity among tillers in winter wheat. J Integr Agric 14:1958–1970. https://doi.org/10.1016/S2095-3119(15)61094-2

Yan L, Loukoianov A, Tranquilli G et al (2003) Positional cloning of the wheat vernalization gene VRN1. Proc Natl Acad Sci U S A 100:6263–6268. https://doi.org/10.1073/pnas.0937399100

Zaharia M, Bolosky WJ, Curtis K, et al (2011) Faster and more accurate sequence alignment with SNAP. arXiv:1111.5572. https://doi.org/10.48550/arXiv.1111.5572

Zhang J, Gizaw SA, Bossolini E et al (2018) Identification and validation of QTL for grain yield and plant water status under contrasting water treatments in fall-sown spring wheats. Theor Appl Genet 131:1741–1759. https://doi.org/10.1007/s00122-018-3111-9

Zhang X, Jia H, Li T et al (2022) TaCol-B5 modifies spike architecture and enhances grain yield in wheat. Science 376:180–183. https://doi.org/10.1126/science.abm0717

Zheng K, Subudhi PK, Domingo J, Magpantay G, Huang N (1995) Rapid DNA isolation for marker assisted selection in rice breeding. Rice Genet Newsl 12:255–257

Publisher's Note Springer Nature remains neutral with regard to jurisdictional claims in published maps and institutional affiliations.

Authors and Affiliations

Tiantian Chen[1] · Kazusa Nishimura[2] · Kazuki Murata[1] · Takanori Yoshikawa[1] · Kyoka Nagasaka[1] · Takahiro Maki[1] · Ko Motoki[2] · Yu Kinoshita[3] · Yu Iwahashi[1] · Hiromo Inoue[1] · Tetsuya Nakazaki[4] · Ryohei Nakano[1]

✉ Kazusa Nishimura
knishimura@okayama-u.ac.jp

✉ Ryohei Nakano
nakano.ryohei.3r@kyoto-u.ac.jp

[1] Graduate School of Agriculture, Kyoto University, 4-2-1 Shiroyamadai, Kizugawa City, Kyoto 619-0218, Japan

[2] Graduate School of Environmental, Life, Natural Science and Technology, Okayama University, 1-1-1 Tsushima-Naka, Kita-Ku, Okayama 700-8530, Japan

[3] Graduate School of Agriculture, Kyoto University, Kitashirakawa Oiwake-Cho, Sakyo-Ku, Kyoto 606-8502, Japan

[4] Office of Institutional Advancement and Communications, Kyoto University, Yoshida-Honmachi, Sakyo-Ku, Kyoto 606-8501, Japan